Accounts

Molecular Magnets Based on Organic Charge Transfer Complexes

Toshiaki Enoki,* Jun-Ichi Yamaura,† and Akira Miyazaki

Department of Chemistry, Tokyo Institute of Technology, Ookayama, Meguro-ku, Tokyo 152

†Institute for Solid State Physics, The University of Tokyo, Roppongi, Minato-ku, Tokyo 106

(Received April 4, 1997)

Organic charge transfer complexes form a large variety of electronic structures from insulating state to metallic state in low-dimensional frameworks, which are governed by the competition between the transfer integral and the on-site Coulomb interaction. In the insulating regime, the generation of localized magnetic moments of π-electron origin provides low-dimensional magnetic systems having the features of quantum spins. The increase in the transfer integral which works to suppress the effect of on-site Coulomb interaction makes π-electrons delocalized, resulting in the appearance of the systems with the coexistence of magnetism and electron transport as materials classified around the Mott–Hubbard boundary. The introduction of localized magnetic moments of *d*-electrons in the complexes gives rise to the interaction between the π-electrons and the magnetic moments of *d*-electrons. Localized magnetic moments of *d*-electrons embedded in insulating complexes are expected to interact with each other through superexchange interaction mediated by the organic π-electron system, while localized *d*-spins in metallic complexes are coupled to each other via the π–*d* interaction, leading to the generation of molecule-based metal magnets. The studies of organic complex-based molecular magnets based on TTF-type donor molecules performed in our group are reviewed.

Magnetism is one of the most essential issues in solid state physics and chemistry, which deals with the behavior of magnetic moments in solids. The behavior of magnetic moments is governed by the competition between the thermal agitation and the interaction working to couple the magnetic moments. From the historical viewpoint, ferromagnetic materials, where magnetic moments are aligned parallel to each other through exchange interaction, have been widely known and interesting for the practical use, leading to the development of various types of ferromagnetic materials. On the other hand, antiferromagnetic materials with antiparallel arrangement of magnetic moments have been attracting physicists due to purely scientific interests, since the absence of spontaneous magnetization, which is caused by the antiparallel spin arrangement, makes antiferromagnetic materials less important from the point of applications. However, the quantum mechanical features of antiferromagnetic spin systems have provided important examples for quantum statistical physics, especially spin systems on low-dimensional frames such as one- or two-dimensional ones. The studies on magnetism up to now have been carried out on the basis of mainly inorganic materials which consist of magnetic moments of transition metal and rare earth metal ions associated with unpaired electron spins in *d*- and *f*-orbitals, respectively, since most organic materials are nonmagnetic except radicals comprising unpaired electrons of molecular origin.

On the contrary to the historical background of magnetism on the basis of inorganic materials, the recent trends in the investigation of organic solids have focused on the functionality of organic materials, whose roots are back to the discovery of organic semiconductors in 1954.[1] Such studies have opened a wide scientific area with a large variety of organic materials having interesting features of electrical conducting properties, magnetic properties, optical properties and so on. In the area of organic solid state science, the field of magnetic organic materials has become prevailed late behind other fields, such as conducting materials and optical materials, because of the difficulty in treating magnetism for chemists who could develop new materials. The recent discovery of an organic ferromagnet *p*-NPNN (=2-(4-nitrophenyl)-4,4,5,5-tetramethyl-4,5-dihydro-1*H*-imidazolyl-1-oxy-3-oxide)[2] has stimulated the investigation of organic magnetic systems, resulting in the development of a large number of organic ferromagnets. At the same time, the developments of organic conductors including organic superconductors[3,4] have provided the bases of the research on molecule-based magnets. The low-dimensionality of the organic solids clearly reveals the favorable features of organic materials as the models of quantum spin systems. Moreover, the cooperation of magnetic moments and conduction carriers in organic conductors is expected to give organic versions of metal magnets. In the

present accounts, we introduce the development of molecular magnets on the basis of charge transfer complexes, which show novel magnetic properties.

Here, we make a brief perspective on the magnetism of organic charge transfer complexes having π-electronic structures. Organic charge transfer complexes consist of electron donors and acceptors, where a π-electron from the HOMO of the donor is transferred to the LUMO of the acceptor. The important structural feature of the organic donors/acceptors is their planar shape, so that the π-electron wave functions that protrude from the molecular plane can easily interact with the wave function of the adjacent molecules. As a consequence, the face-to-face molecular configuration, which is stabilized through the intermolecular interaction associated with the overlap of the π-orbitals, gives the molecular stacking arrangements resulting in the formation of a one- or two-dimensional lattice. Figure 1 shows a schematic model of the molecular arrangement with the one-dimensional structure, which is characterized with one π-electron for each HOMO/LUMO state of donor/acceptor (half-filled state) for simplicity. From the physical viewpoint, the electronic structure of the molecular arrangement is explained in terms of one-dimensional electronic system with the transfer integral t and the on-site Coulomb repulsion U between two electrons, the latter of which works when these are on the same molecule. The transfer integral t is defined for the intermolecular interaction as given by the following equation:

$$t = \int \psi_i(x)^* H \psi_{i+1}(x) \mathrm{d}x, \quad (1)$$

where H is the Hamiltonian for the one electron term, and $\psi_i(x)$ is the wave function for molecular site i. The on-site Coulomb interaction U is roughly described in terms of the dielectric constant ε and the distance between two electrons r as expressed by

$$U = e^2/\varepsilon r, \quad (2)$$

where r is scaled to the size of the molecule on which the two electrons are staying. The transfer integral that works to hop an electron from one molecule to the neighboring molecule gives the mobile feature of electrons, while the on-site Coulomb interaction makes it suppressed. As a consequence, the electronic structure of the system is governed by the competition between t and U, which varies from metallic to insulating state depending on the ratio of t/U. Namely, the increase in the ratio favors metallic states, whereas the decrease stabilizes insulating states. The important roles of these two parameters in the electronic structures can be easily seen on the basis of the combination between the molecular orbital scheme and Heitler–London scheme. Figure 2 explains the change in the electronic structures depending on the ratio t/U in relation to these two schemes with a dimer model of acceptor molecules having one electron in their LUMO. In the Heitler–London scheme with a large U, where an electron is localized in each donor molecule, the hopping of an electron from one molecule to the other requires the energy of U. Therefore, each acceptor in the ground state possesses one localized electron with a magnetic moment, which is well stabilized by the large excitation energy of U. On the other hand, the molecular orbital regime with large transfer integral t gives a delocalized electronic structure, where two electrons are well delocalized in the dimer unit, resulting in the disappearance of net magnetic moments due to the antiparallel coupling of the spins of the two electrons occupying the same molecular orbital. The intermediate region between the Heitler–London limit and the molecular orbital limit is described in terms of the two parameters t and U. The ground state of the Heitler–London scheme is split into two states due to the perturbation of t, where the energy splitting is given by $2t^2/U$. The competition between t and U gives any electronic structure ranging between the two limiting cases in actual organic molecules. The concept of electronic structures obtained on the basis of the dimer model is generalized to bulk solids of organic charge transfer complexes. The Heitler–London limit $t/U \longrightarrow 0$ corresponds to the insulating state with localized magnetic moments, which is called a Mott insulator in the solid state physics language,

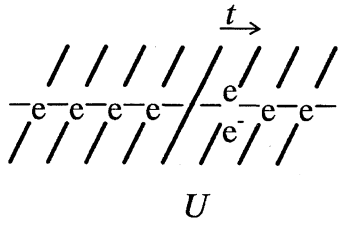

Fig. 1. Schematic model of a one-dimensional electronic system comprising the stacking of planar organic molecules where each molecule has a half-filled state except the molecules related to the electron transfer process. The transfer integral and the on-site Coulomb interaction are denoted by t and U. The hopping of an electron requires the energy elevation of U.

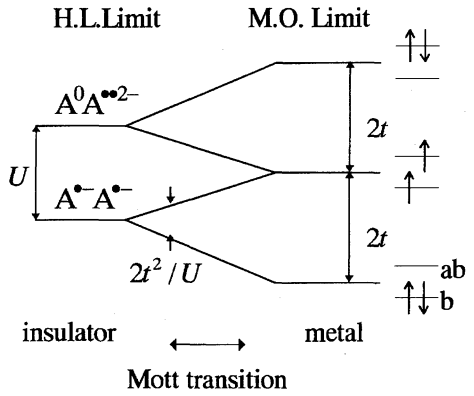

Fig. 2. Schematic model of the electronic state of a dimerized acceptor unit AA, which can be generalized to the electronic structure of a bulk system. H. L. limit and M. O. Limit denote the Heitler–London limit and the molecular orbital limit, respectively. The transfer integral and the on-site Coulomb interaction are given by t and U, respectively, while b and ab represent the bonding and antibonding molecular orbitals, respectively, in the molecular orbital scheme. In the case of the donor system, the equivalent model is resulted by replacing electrons with holes.

whereas the molecular orbital limit $t/U \longrightarrow \infty$ gives a metallic state with the absence of localized magnetic moments. The interesting feature is the presence of the boundary between the insulator state and the metallic state, which is called the Mott–Hubbard boundary. A change of temperature or pressure which modifies the transfer integral as an intermolecular-distance-sensitive parameter can make organic complexes pass from the metallic state to the insulator state, resulting in the metal-insulator transition (Mott transition).

The strategies for the development of organic complex-based molecular magnets appear under the schemes with t and U, which are categorized into three classes. In the case of small t/U, localized magnetic moments are generated on organic molecules which form a low-dimensional magnetic lattice such as a one- or two-dimensional lattice. The overlap of wave functions between electrons on the adjacent molecules makes antiparallel spin arrangement, giving antiferromagnetic interaction with the strength of $J \approx t^2/U$. Moreover, organic molecules consisting of light elements such as C, H or S have small spin-orbit interaction, so that the magnetic anisotropy whose main origin is eventually the dipole–dipole interaction is considerably small. Consequently, the complexes in this case are characterized basically as low-dimensional Heisenberg antiferromagnetic systems with the features of quantum spins, where the exchange interaction is isotropic as described in the following equation:

$$H = -2J\boldsymbol{S}_i\boldsymbol{S}_j, \tag{3}$$

with spin operator $\boldsymbol{S}_i$ at site i. The second category is the case with the intermediate strength of t/U around the Mott–Hubbard boundary, where the features of metallic state and insulator state coexist. We can realize the coexistence of localized magnetic moments and metallic electron transport. The correlation between magnetism and electron transport provides attractive contemporary topics in this regime. The case with a large t/U gives the third category belonging to metallic states. Since there is the absence of localized magnetic moments of π-electrons, we need to introduce foreign magnetic species having localized magnetic moments in this case. The introduction of magnetic ions with d- or f-electrons as a counterpart for an organic donor or acceptor is employed for the development of organic complex-based magnets. In this case, π-conduction carriers work to mediate the exchange interaction between the localized magnetic moments of d-electrons, where the π–d interaction brings about the molecular version of metal magnets, in contrast to ordinary inorganic metallic magnetic systems with transition metals realized through the s–d interaction. The low-dimensional metallic systems occasionally tend to be changed to insulating states due to the instability (Peierls instability) inherited to the low-dimensionality in their electronic structures. Even in such cases, π-electrons work to couple the magnetic moments of d-electrons through the superexchange mechanism.

Under the viewpoint on molecular based magnets mentioned above, we have investigated the magnetic properties of organic complex-based molecular magnets with the employment of TTF-type organic donors; BEDT-TTF, C_1TET-TTF, and M(dddt)$_2$ listed in Fig. 3. The present accounts introduce some studies on organic complex-based molecular magnets in our group. In Section 1, the discussion is devoted to the materials classified in the first and second categories; β'-(BEDT-TTF)$_2$X (X=ICl_2, $AuCl_2$), (C_1TET-TTF)$_2$Br, and (BEDT-TTF)$_2$Br·CH_2(OH)CH_2OH. β'-(BEDT-TTF)$_2$X (X=ICl_2, $AuCl_2$) show the features of two-dimensional square lattice Heisenberg antiferromagnets. In (C_1TET-TTF)$_2$Br, spin frustration affects magnetic behavior as a two-dimensional triangular Heisenberg antiferromagnetic system. (BEDT-TTF)$_2$Br·CH_2(OH)CH_2OH is revealed to be located around the Mott–Hubbard boundary with the coexistence of magnetism and electron transport. In Section 2, we discuss the systems with localized magnetic moments of d-electron in the third category. C_1TET-TTF·$FeBr_4$, [Ni(dddt)$_2$]$_3$(FeX_4)$_2$ (X=Cl, Br) and [M(dddt)$_2$]$_2$$FeX_4$ (M=Pd, Pt, Au; X=Br) undergo three-dimensional magnetic long range order through the π-electron-mediated superexchange interaction. In (BEDT-TTF)$_3$$CuBr_4$ the cooperation of d-localized magnetic moments and π-conduction carriers gives a novel correlation between magnetism and electron transport through the π–d interaction. The conclusion is given in Section 3 with comments on the future prospects of the organic complex-based magnets.

1. π-Electron-Based Magnets

1-1. Two-Dimensional Magnetic Systems. The low-dimensional structures of TTF-based organic charge transfer

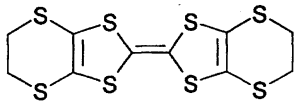

BEDT-TTF

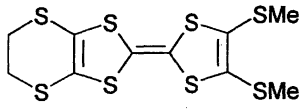

C_1TET-TTF

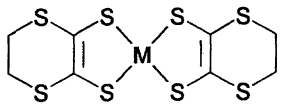

M(dddt)$_2$

Fig. 3. Structures of TTF-type donor molecules; BEDT-TTF (bis(ethylenedithio)tetrathiafulvalene), C_1TET-TTF (bis(thiomethyl)ethylenedithiotetrathiafulvalene), M(dddt)$_2$-(M=Ni, Pd, Pt, Au; H_2dddt=5,6-dihydro-2,3-dimercapto-1, 4-dithiin).

complexes give low-dimensionality in their magnetic properties. In addition to this, magnetic moments of π-electrons (S=1/2) on organic molecules are considered to characterize the magnetic systems as low-dimensional Heisenberg antiferromagnets with the features of quantum spins, taking into account the absence of strong magnetic anisotropy due to the spin-orbit interaction. Here, we discuss two kinds of magnetic systems classified in two-dimensional antiferromagnetic systems; β'-(BEDT-TTF)$_2$X (X=ICl_2, $AuCl_2$)[5] and (C_1TET-TTF)$_2$Br.[6]

β'-(BEDT-TTF)$_2$X (X = ICl_2, $AuCl_2$) with space group $P\bar{1}$ have quasi-one-dimensional isostructural crystal structures,[7–11] where intermolecular side-by-side S···S atomic contacts between BEDT-TTF molecules play a role in the formation of linear chains of dimerized BEDT-TTF molecules oriented parallel to the b-axis. The face-to-face S···S atomic contacts, which are relatively weak in comparison with the side-by-side interactions, give two-dimensional arrays of the linear chains in the bc-plane which are separated from each other through an anion layer.[8] This structural feature suggests the quasi-two-dimensionality in the electronic structure, as supported by the extended Hückel band calculation[12] showing a metallic state. Electrical resistivity behaves as a semiconductor with a large activation energy $E_A \approx 0.12$ eV for both ICl_2 and $AuCl_2$ salts, in contradiction to the band structure prediction. The magnetic susceptibility proves the presence of localized magnetic moments with S=1/2 per BEDT-TTF dimer unit. Consequently, the complexes are classified among Mott insulators, whose magnetic systems are characterized as quasi-two-dimensional Heisenberg antiferromagnets with the presence of intra- and inter-chain exchange interactions J_b, J_c. Figure 4 shows the temperature dependence of magnetic susceptibility for the ICl_2 salt. The magnetic susceptibility of the $AuCl_2$ salt has a trend in the behavior of temperature dependence similar to that of the ICl_2 salt. Namely, it has a broad peak around 110 K which is suggestive of the development of magnetic short range order for both salts, and then it has a discontinuous change at an onset temperature of T_N=22 and 28 K for three-dimensional long range order in the ICl_2 and $AuCl_2$ salts, respectively. The strengths of the intra- and inter-chain exchange interactions in the two-dimensional layers are roughly estimated based on the extended Hückel electronic structure calculation, taking into account the relation between the transfer integral and the exchange interaction $J \propto t^2$. The estimate gives the ratio of the exchange interactions $J_c/J_b \approx 0.5$, where the numbers of neighboring spins are given to be z_c=2 and z_b=2 from the numbers of transfer integrals connecting neighboring donor dimer units. Theoretical fitting[13] to the observed magnetic susceptibility gives the rough estimate of the exchange interaction J=59 K for both the ICl_2 and $AuCl_2$ salts, assuming that the magnetic lattices are characterized as two-dimensional square lattices with $J_b=J_c=J$. The calculation of interlayer interaction J' based on the Green function method[14] that relates J' with J and T_N gives $J'/J \approx 10^{-4}$ and 10^{-3} for the ICl_2 and $AuCl_2$ salts, respectively. The structural trend that the inter-layer distance

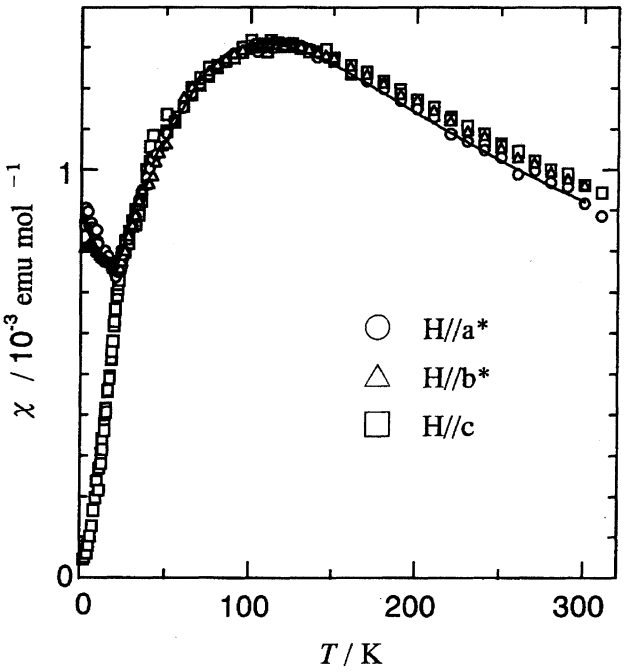

Fig. 4. Temperature dependence of the susceptibility of β'-(BEDT-TTF)$_2$$ICl_2$ in the field parallel to the three crystallographic axes. A solid line denotes the best fitting for the two-dimensional square lattice Heisenberg antiferromagnet model.[13]

is shortened by 1.32% as we change anions from larger ICl_2 to smaller $AuCl_2$ is in good agreement with the change in the strengths of the inter-layer exchange interactions. The appearance of anisotropy in the magnetic susceptibility below T_N shows that the easy spin axis is oriented parallel to the c-axis. In Fig. 5 are shown the magnetization curves at 2.0 K for the ICl_2 salt. A spin-flop transition is observed at H_{sf}=1.1 T when the magnetic field is applied parallel to the c-axis, in good agreement with the spin axis suggested by the anisotropy of the magnetic susceptibility. The spin-flop field H_{sf} is related to the exchange field H_E and anisotropy field H_A through the relation;

$$H_{sf} = \sqrt{H_A(2H_E - H_A)} \,. \quad (4)$$

Using the value of H_E obtained from the exchange interaction J and H_{sf}, we estimate the anisotropy field $H_A/H_E \approx 2.0 \times 10^{-5}$. The small anisotropy field is considered to be caused by the dipole–dipole interaction,[15] consistent with the features of the Heisenberg spin system.

Next, we discuss the magnetism of (C_1TET-TTF)$_2$Br. (C_1TET-TTF)$_2$Br is a novel organic cation radical salt characterized in terms of the charge localization and low-dimensional magnetism of localized π-electrons on the donor molecules.[6] Figure 6 shows the crystal structure and the overlap integrals of (C_1TET-TTF)$_2$Br. Since all donor molecules are crystallographically equivalent, they are expected to have the same partial charge +0.5 taking into account the stoichiometry of 2 : 1. C_1TET-TTF donors form a two-dimensional lattice in the bc-plane, where the donor arrangement has zigzag feature with a head-to-tail configuration in the in-

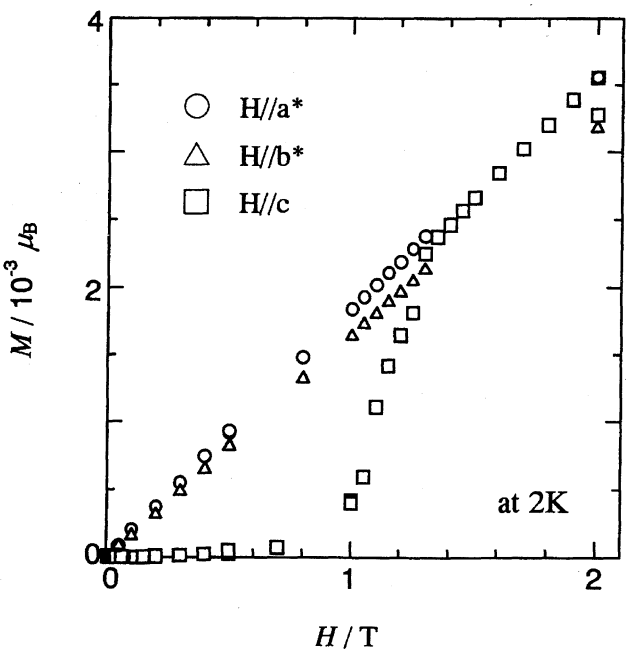

Fig. 5. The magnetization curves of β'-(BEDT-TTF)$_2$ICl$_2$ at 2 K in the field parallel to the three crystallographic axes.

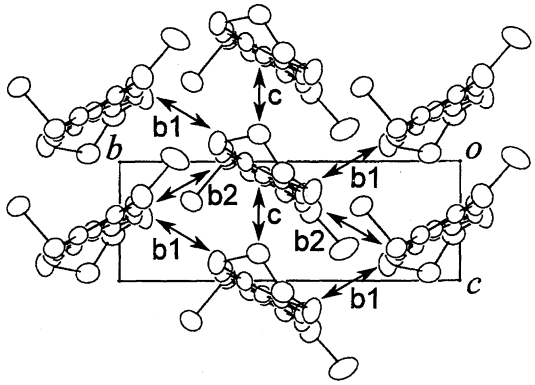

Fig. 6. Crystal structure of (C$_1$TET-TTF)$_2$Br and the overlap integrals which are $b1$=5.4, $b2$=4.3 and c=5.8×10^{-3} in the bc-plane.

terstack direction. The overlap integrals of the donor HOMO calculated by extended Hückel method[12] are given to be $b1$=5.4, $b2$=4.3, and c=5.8×10^{-3}, which reveals a two-dimensional character with small differences in the strengths of the transfer integrals. Figure 7 shows the band structure and the Fermi surfaces calculated with the tight binding method.[12] The band calculation suggests the presence of two-dimensional metallic bands which have the narrow band widths in the range of 0.4 eV due to the small overlap integrals. Since the degeneracy in the M–Y dispersion is caused by the crystallographic symmetry, the 3/4-filled nature is intrinsic. On the other hand, the first Brillouin zone has the half-filled feature, taking into account the Harrison's simple band construction.[16] The electrical resistivity behaves semiconductively with an activation energy of E_A=0.2 eV and the room temperature resistivity value of ρ_{RT}=40 Ω cm. This result is in disagreement with the band calculation that

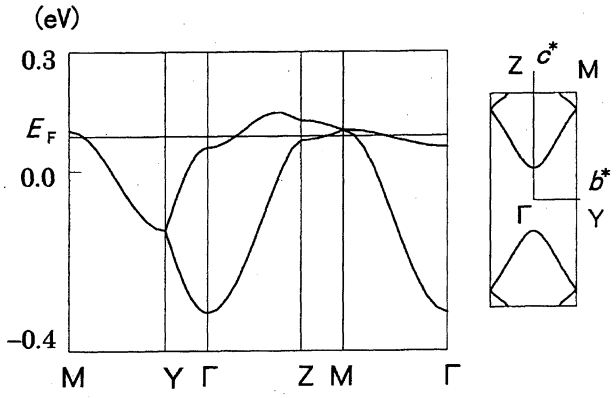

Fig. 7. Band structure and Fermi surfaces of (C$_1$TET-TTF)$_2$Br. The energy scale is given on the basis of donor HOMO energy (−10 eV).

suggests a metallic behavior.

Figure 8 represents the temperature dependence of the magnetic susceptibility in the applied field parallel to the b-axis. The susceptibility shows the Curie–Weiss behavior in the high temperature range, and then it indicates a broad hump of low-dimensional antiferromagnetic short range order around 12 K. The susceptibility data in the field parallel to the a^*, b, and c-axes are well represented by the sum of a Curie–Weiss term and a temperature independent one after the correction of the Pascal diamagnetic contribution above 30 K. The Curie constant C, the antiferromag-

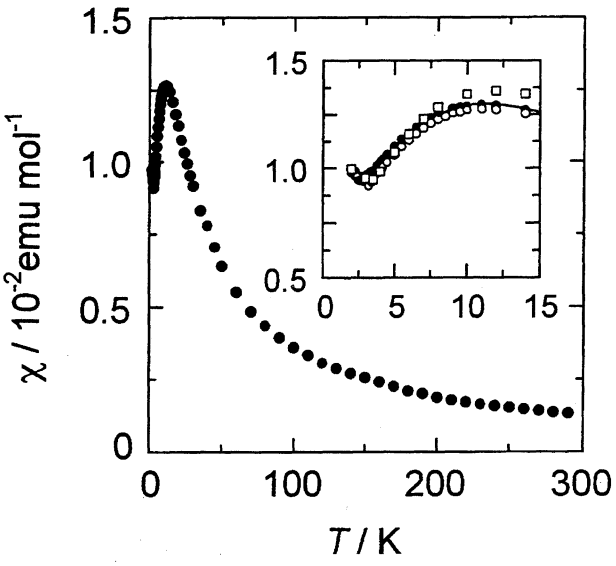

Fig. 8. Temperature dependence of the magnetic susceptibility in the applied field of H=1 T parallel to the b-axis. The inset shows the temperature dependence of magnetic susceptibility below 30 K in the applied field parallel to the a^* (●), b (○), and c (□)-axes. The theoretical fitting (solid line) for the two-dimensional square lattice Heisenberg antiferromagnet model[13] in the temperature range 8—290 K gives the exchange interaction of J=−6.1 K, where 0.5 spin with S=1/2 is allotted to one C$_1$TET-TTF donor according to the charge distribution. An antiferromagnetic transition is observed at T_N=3 K.

netic Weiss temperature Θ, and the temperature independent diamagnetic susceptibility χ_0 are estimated at C=0.454 emu K mol^{-1}, Θ=−17.3 K, and χ_0=−1.1×10^{-4} emu mol^{-1}, respectively, where the mole unit involves one formula unit (C_1TET-TTF)$_2$Br. From the Curie constant, the spin density N (S=1/2) is estimated at N=1.2 spin mol^{-1} using the ESR g-value, suggesting the existence of one localized magnetic moment of S=1/2 in two donors. The detailed susceptibility is exhibited in the inset of Fig. 8 in the low temperature region below 30 K in the applied field parallel to the a^*, b, and c-axes. Below 3 K the susceptibility shows an abrupt increase irrespective of field direction. The behavior of the susceptibility and the ESR line width broadening in the low temperature range suggest the onset of an antiferromagnetic order at T_N=3 K. However, it is worth noting the absence of magnetic anisotropy below T_N among the susceptibilities in the field applied parallel to the three independent crystallographic axes. Moreover, magnetization curves in the field parallel to the a^*, b, and c-axes at 2 K up to 5 T show a slight concavity with the absence of an apparent spin-flop transition.

Let us now discuss the feature of the charge localization on the donor molecules in this compound. The semiconductive behavior with a large activation energy and the presence of localized magnetic moments on C_1TET-TTF donors suggest features of a Mott insulator generated by the competition between the on-site Coulomb interaction and the transfer integral. Comparison to the reported BEDT-TTF-based Mott insulators[5,17–21] provides an important suggestion on the electronic structure of the present compound. For instance, α' and β'-(BEDT-TTF)$_2$X type Mott insulators have intrinsic half-filled bands realized by the band splitting due to the strong donor dimerization. In these salts, the competition between the interdimer transfer integral and the effective on-site Coulomb interaction, the latter of which is given by the intradimer transfer integral,[22] generates the Mott insulating state, where the magnetic moment is well localized around the region confined in the dimerized unit of BEDT-TTF molecules. On the other hand, the present compound has the intrinsic 3/4-filled band structure due to the uniform donor stacking, indicating that it is not likely to be an ordinary Mott insulator, although it has the half-filled band structure in the first Brillouin zone, as shown in Fig. 7. In this sense, the picture of the donor-dimer-based Mott insulating state seems to fail here; thus, a localized moment is thought to be extended widely over a unit cell. Consequently, the features of the electron localization are considered to be situated far from Mott insulators in the ordinary BEDT-TTF complexes, demonstrating that the present compound lies just around the Mott boundary. Moreover, it is suggested that this less localized nature affects the magnetic behavior in (C_1TET-TTF)$_2$Br.

Now, we move on to the discussion on the magnetic structure and the exchange interaction mechanism in details. Taking into account the result that all donor molecules are crystallographically equivalent, all the donor molecules are equally charged due to the charge transfer to anions. Thus, we assume that 0.5 spin with S=1/2 exists on each donor molecule within the consideration of the X-ray average structure, although the underlying physics behind it remains to be clarified. The antiferromagnetic exchange interaction $J \approx t^2/U$ between the donor molecules is described in terms of the transfer integral t and the on-site Coulomb interaction U. From the result of the extended Hückel calculation, the ratio of the exchange interactions is given to be $J_2/J_1 \approx 0.5$, where the exchange interactions are estimated by $J_1 \approx t_{b1}{}^2/U \approx t_c{}^2/U$ and $J_2 \approx t_{b2}{}^2/U$ for magnetic neighbors. Therefore, the exchange interaction network is characterized as a distorted triangular lattice with the stronger interaction J_1 and the weaker interaction J_2, as shown in Fig. 9. In the case of $J_1=J_2$ the magnetic system is regarded as a two-dimensional regular triangular lattice antiferromagnet, where the next nearest neighbor of a magnetic site becomes involved in the nearest neighbors of the magnetic site. In the regular triangular structure consisting of three magnetic sublattices, the antiferromagnetic interaction causes a frustration feature in the spin arrangement, which provides interesting models for classical and quantum spins.[23,24] Actually, in such a case, an antiparallel spin arrangement between two sublattices makes spins on the remaining sublattice frustrated; in other words, the antiparallel coupling of two spins is achieved at the expense of the energy stabilization of the spins which do not participate in the antiparallel spin arrangement. Meanwhile, in the present case having $J_1 > J_2$, the magnetic lattice is expected to be the distorted triangular one. Here, we analyze the susceptibility with a hump at 12 K by means of the two-dimensional square lattice antiferromagnetic Heisenberg model[13] only with predominant exchange constant J_1 in order to find out the features of the spin frustration. As a result, the susceptibility is well described by the two-dimensional square lattice Heisenberg antiferromagnet model with the exchange energy of J_1=−6.1 K. It is worth recalling that the estimated exchange interaction is one order of magnitude lower than the exchange interactions of α', β'-(BEDT-TTF)$_2$X[5,25] and θ-(BEDT-TTF)$_2$Cu$_2$(CN)[N(CN)$_2$]$_2$ salts.[26] Actually, the transfer integral between the adjacent dimers in α' and β'-(BEDT-TTF)$_2$X salts, which have a two-dimensional square antiferromagnetic lattice of the dimerized

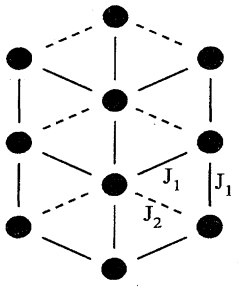

Fig. 9. Schematic representation of the triangular magnetic lattice for the C_1TET-TTF layer with antiferromagnetic interactions J_1 and J_2, where the ratio of the interactions is estimated at $J_2/J_1 \approx 0.5$. Solid circle denotes the donor molecule which is regarded as the site having 0.5 spin of S=1/2.

donors having $S=1/2$,[5,18–20] is in the same range as the transfer integrals of the present compound in spite of the large difference in the magnitudes of the exchange interactions. Furthermore, θ-(BEDT-TTF)$_2$Cu$_2$(CN)[N(CN)$_2$]$_2$, in which the transfer integral is also in the same range, forms a similar distorted triangular antiferromagnetic lattice[26] to that of the present compound. In this salt, the ratio of the exchange interactions estimated at $J_2/J_1=0.1$ is considerably smaller than that in the present compound, suggesting that the predominance of J_1 makes the spin frustration considerably depressed. Consequently, the apparent decrease of the estimated exchange interaction in the present compound is proved to be associated with the frustrated spin arrangement through the competition between the antiferromagnetic interactions J_1 and J_2. In relation to the feature of spin frustration, the ordered state below T_N is considered to be characterized as the z_2 vortex state in the triangular antiferromagnetic system with quantum spins,[23,27,28] judging from the absence of magnetic anisotropy shown in Fig. 8 in addition to the concave feature of the magnetization curve. It is also worth pointing out the importance of the novel electronic structure related to the magnetic features. That is, the less localized nature in the electronic structure, as discussed before, may cause the reduction in the strengths of exchange interactions, in comparison with the ordinary organic Mott insulators that have well localized magnetic moments on donor molecules.

1-2. Magnetic System Around the Mott–Hubbard Boundary. As in the examples presented in the preceding section, radical ion salts with the stoichiometry of 2 : 1 provide a useful target for examining the physical properties with varying the t/U ratio. In these salts, the donor molecules have a tendency to form dimers as in the case of β'-(BEDT-TTF)$_2$ICl$_2$,[5] and in this case the effective on-site Coulomb repulsion U_{eff} is expressed approximately as $U_{eff}\approx 2|t_{intra}|$, where t_{intra} is the intradimer transfer integral.[22] The t/U ratio is therefore governed only by the ratio of t_{inter}/t_{intra} (t_{inter}: interdimer transfer integral), which can be regulated by chemical modification such as anion and/or solvent substitution. To date, chloride and bromide salts of BEDT-TTF are found only in the coexistence of neutral solvent molecules, such as H_2O, incorporated within the crystal.[29–32] In such salts, an anion-solvent molecule network is formed with the aids of the hydrogen-bonds between the anions and the neutral molecules. This means that the solvated salts of BEDT-TTF can be good candidates for our present purpose, as the solvent substitution will lead to the modification of the t_{inter}/t_{intra} ratio.

(BEDT-TTF)$_2$Br·CH$_2$(OH)CH$_2$OH crystallizes in a space group $P2_1/n$.[33] at room temperature. In the crystal two donor molecules are aligned in parallel to form a face-to-face dimer; such dimers are then stacked along the a-axis to make a column, as exhibited in Fig. 10. The intradimer overlap integrals are more than 5 times larger than the interdimer overlaps, which leads to the strong electron correlation. Since the long axes of donor molecules in the adjacent dimers facing each other are aligned obliquely, the strengths of the interdimer overlap integrals along the a-axis are about a half of

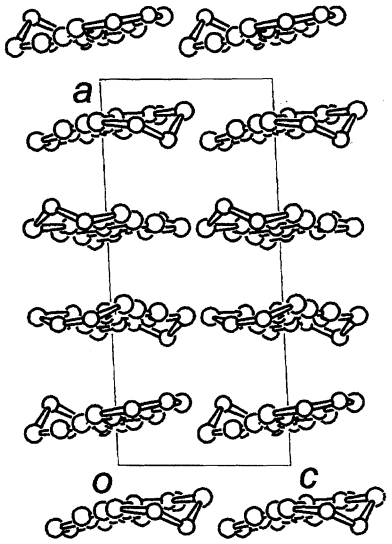

Fig. 10. Crystal structure of BEDT-TTF$_2$Br·CH$_2$(OH)-CH$_2$OH at room temperature viewed along the b-axis. For simplicity, only donor molecules located around $y\approx 0$ are drawn. Hydrogen atoms, anions and solvents are also omitted.

those along the c-axis, which makes the electronic system of the salt quasi-one-dimensional. Between the adjacent donor sheets, the bromide anions and the ethylene glycol molecules form hydrogen-bonded chains, where the solvent molecules are conformationally disordered.[33]

Around room temperature this salt behaves as a metal, with the room temperature resistivity of 0.6 Ω cm along the c-axis as shown in Fig. 11, where weak temperature dependence in the resistivity above 200 K suggests the effect of the electron correlation.[34] The metallic behavior is consistent with the results of the band structure calculation based on the room-temperature crystal structure using the tight-binding approximation with the extended Hückel Hamiltonian.[12] Within the first Brillouin zone, there are two pairs of one-

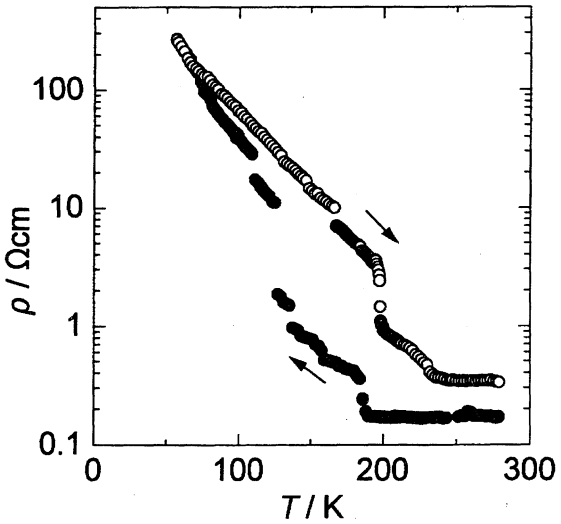

Fig. 11. Temperature dependence of the resistivity of BEDT-TTF$_2$Br·CH$_2$(OH)CH$_2$OH measured along the c-axis; ● - temperature decreasing, ○ - temperature increasing.

dimensional warped Fermi surfaces, predicting the metallic behavior. When one decreases the temperature with the cooling rate of 1 K min^{-1}, there is a resistivity jump at 185 K, and below this temperature the salt becomes a semiconductor with an activation energy of E_A=350 K. During the heating process with a similar heating rate, the discontinuity of the resistivity appears at 195 K. Thus there is a first order phase transition at T_{c1}=190 K accompanied by hysteresis with the temperature difference of 10 K, which is also confirmed with the detection of latent heat (3.21 kJ mol^{-1}) by DSC measurement.

Despite the metallic behavior in the conductivity, the static susceptibility has a character of the localized magnetic moments even above about 200 K, as shown in Fig. 12.[34] This fact demonstrates that the high temperature phase above T_{c1} is characterized as a highly correlated metal with the coexistence of magnetism and electron transport. The value of susceptibility at room temperature is 1.1×10^{-3} emu mol^{-1}, which is one order of magnitude larger than the values for ordinary metallic BEDT-TTF salts, such as (BEDT-TTF)$_2$ClO$_4$·(CHCl$_2$CH$_2$Cl)$_{0.5}$ (4.2×10^{-4} emu mol^{-1}).[35] The susceptibility obeys the Curie–Weiss law with the antiferromagnetic Weiss temperature Θ=−83 K. From the value of the Curie constant, the spin concentration is estimated at one spin S=1/2 per BEDT-TTF donor dimer, in good agreement with the one expected from the stoichiometry of 2 : 1 on the basis of the localized spin model. The susceptibility drops abruptly by one half at T_{c1} with a hysteretic behavior, consistent with the result of the resistivity measurement. Below T_{c1}, where the salt becomes semiconductive, the susceptibility gradually decreases according to the temperature decrease. Since the Bonner–Fisher one-dimensional Heisenberg model[36] or the alternating-chain model[37] does not explain the experimental data well enough, the origin of this behavior is not well characterized yet. However, judging from the crystal structure, it may be reasonable to think that this gradual decrease in the susceptibility is related to the low-dimensional feature of the localized spin system as a result of the transition at T_{c1}. At T_{c2}=80 K it drops again with the exponential decay toward zero as the temperature decreases. The absence of hysteresis around T_{c2} indicates the onset of a second order phase transition. The exponentially decaying behavior below T_{c2} shows the singlet ground state of this system with a magnetic gap of 120 K.

The results of ESR measurements characterize the phase transition around T_{c1} as a structural transition accompanied with the orientational change of the donor molecules. The ESR signal shows a Lorentzian shape with g=2.0025 and the peak-to-peak line width $\Delta H\approx1$ mT. The line width is smaller than that of ordinary metallic BEDT-TTF salts (e.g. (BEDT-TTF)$_3$HSO$_4$: 5—7 mT),[38] but rather close to semiconductive ones (e.g. β'-(BEDT-TTF)$_2$ICl$_2$: 1 mT).[5] On lowering the temperature, the line width decreases gradually in the metallic phase, and at T_{c1} it increases discontinuously about 40%. At this point the g-value for $H//a$-axis leaps from 2.0025 to 2.0030, which corresponds to the molecular rotation of ca. 1°. Consequently, the phase transition at T_{c1} is found to involve a structural transformation accompanied with the orientational change of the donor molecules. On the other hand, there is no significant change in the g-values at T_{c2}, and below this temperature the line width decreases monotonously as the temperature decreases. Therefore, the structural change at T_{c2} is a subtle one even if it exists, which is consistent with the second-order nature of the transition.

The most interesting property of this material is the angular dependence of the ESR line width as given in Fig. 13.[39]

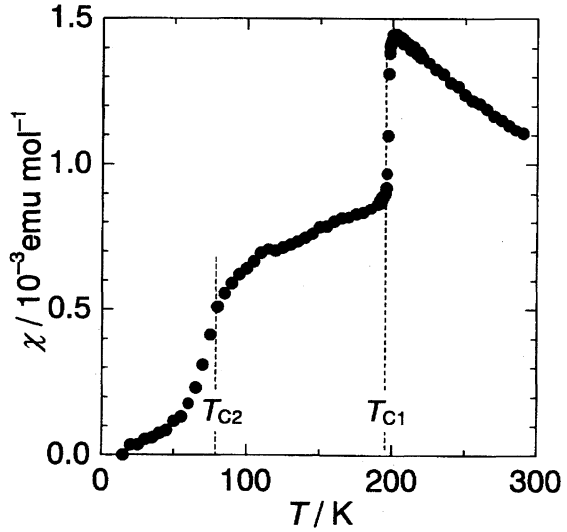

Fig. 12. Temperature dependence of the static magnetic susceptibility of BEDT-TTF$_2$Br·CH$_2$(OH)CH$_2$OH for heating process. Two phase transition points, T_{c1} and T_{c2}, are also shown at 190 and 80 K, respectively.

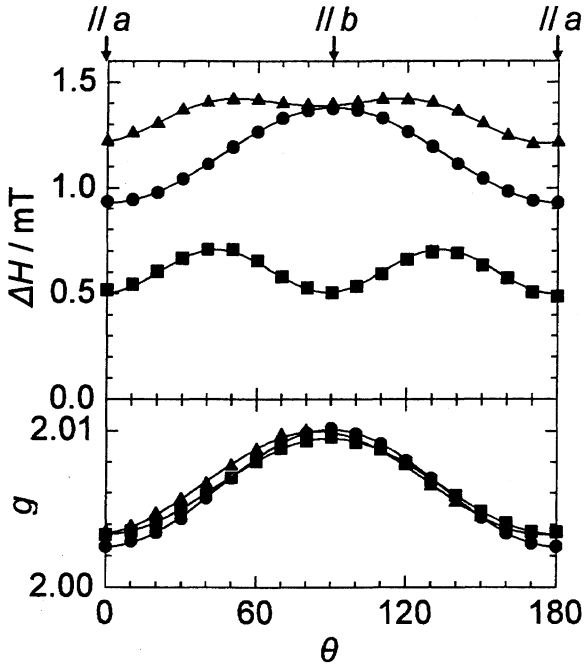

Fig. 13. Angular dependence around the c-axis of the ESR peak-to-peak line width (top) and the g-value (bottom) of BEDT-TTF$_2$Br·CH$_2$(OH)CH$_2$OH at 280 K (●), 150 K (▲), and 60 K (■).

In the metallic regime, both the g-value and the line width have ordinary sinusoidal angular dependence, with a maximum appearing in the external field applied along the b-axis. Below T_{c1}, however, two maxima of the line width emerge when the sample is rotated around the c-axis. When the temperature of the sample is lowered down to 60 K, the mean value of the line width decreases, and the positions of the maxima are shifted so that the line width has the periodicity of roughly 90°. Obviously this double-maximum feature does not come solely from the lattice low-dimensionality, which should show the maxima at the magic angle (54.7°).[40] In addition, the ESR line width can not be explained from the magnetic dipole–dipole interaction. Using the second moment method, the dipolar line width along the b-axis is estimated at 21 mT, which is 15 times larger than the experimental value, suggesting the presence of an exchange narrowing effect. The anomalous angular dependence of the line width, which cannot be explained only by the dipole–dipole interaction, demonstrates the important role of the anisotropic exchange interaction that contributes to adding a trace of Ising spin characteristics in the magnetic system.[41] The detailed analysis based on this line is now in progress.

2. π–d Interaction Systems

2-1. Molecular Magnets with π-Electron-Mediated Superexchange Interactions. For the realization of novel physical properties based on the π–d interaction, a number of radical ion salts containing metal halide anions as counter anions have been developed.[19,42–56] Most of them show, however, little interaction between magnetic anions. Their magnetic susceptibility just obeys the Curie–Weiss law with a small absolute value of the Weiss temperature, and no magnetic ordering such as ferro- or antiferromagnetic transition is observed. Two remarkable exceptions are (BEDT-TTF)$_3$CuBr$_4$ and λ-(BEDT-TSF)$_2$FeCl$_4$.[57] The next section is devoted to the details of the former salt. In the latter salt, an antiferromagnetic transition drives the onset of a metal-insulator transition at T_c=8 K. In order to develop π–d interacting systems, there are several things to be considered. Firstly, the d-electrons of the counter anion should be sufficiently delocalized to the ligand atoms. Secondly, there should be close contacts between the ligand of the counter anion and the chalcogen atoms of donor molecules. These two points can be good guiding principles for selecting the donor and anion molecules for realizing the π–d system.

As counter anions, we mainly employ FeX_4^- and CuX_4^{2-} anions (X=Cl, Br) for the following reasons. Comparing antiferromagnetic transition temperatures and the Weiss temperatures of 3d transition metal halides MX_2 (M=Mn, Fe, Co, Ni, Cu; X=F, Cl, Br, I), the magnetic interaction between d-electrons is stronger in order of Mn<Fe<Co<Ni<Cu and F<Cl<Br<I.[58] Especially, $CuBr_2$ has a remarkably large exchange interaction between the localized spins, due to the spin polarization largely extended to ligand bromine atoms caused by the delocalized feature of d-electrons on the copper atom, suggesting the advantage of using $CuBr_4^{2-}$ as a counter anion. From the practical aspects in sample preparation, however, this anion exists in the solution only under the high concentration of Br^-;[59] hence Br^- salt tends to be stabilized instead of desired $CuBr_4^{2-}$ salt. This situation makes the preparation of $CuBr_4$ salts rather difficult except for the case of (BEDT-TTF)$_3$CuBr$_4$. On the other hand, FeX_4^- ions are relatively stable and are easily handled in the preparation of complexes. In addition, it is possible to replace the anion with diamagnetic GaX_4^- anion without changing the crystal structure,[60,61] which is useful to clarify the role of π-spins on the donor in these systems.

Here, we introduce the π–d systems obtained between FeX_4^- and two kinds of TTF-type donors C_1TET-TTF and M(dddt)$_2$. As the first example, we investigate FeX_4 (X=Cl, Br) salts of C_1TET-TTF, expecting the emergence of the close inter-molecular atomic contacts between donors and magnetic anions by making use of the unshared electron pairs of the sulfur atoms of the flexible methylthio groups.[19,49] These salts are isostructural to each other with the 1 : 1 stoichiometry, regardless of the counter anion. Figure 14 presents the unit cell of the representative salt C_1TET-TTF·FeBr$_4$ projected on the [1 0 $\bar{1}$] plane. The donor molecules forming a head-to-tail dimer are stacked along the c-axis. The molecular axes of the adjacent dimers cross nearly orthogonally and there are no close side-by-side S···S contacts between the adjacent donor molecule dimers, suggesting that direct interaction between donors is negligibly weak. Two adjacent $FeBr_4^-$ anions are related with the twofold screw symmetry, and the counter anions form zigzag chains through X···X contacts, whose distances (Br···Br: 3.783(2), Cl···Cl: 3.67 Å) are close to the twice the van der Waals radii (Br···Br: 3.80, Cl···Cl: 3.67 Å).[62] Since the X···X distances between the chains (Br···Br: 4.301(4), Cl···Cl: 4.48 Å) are longer than that in a chain, direct interactions between anion chains are considered to be negligible. On the other hand, there are a number of close X···S contacts between the counter anion and the six-membered ring of the donor, whose dis-

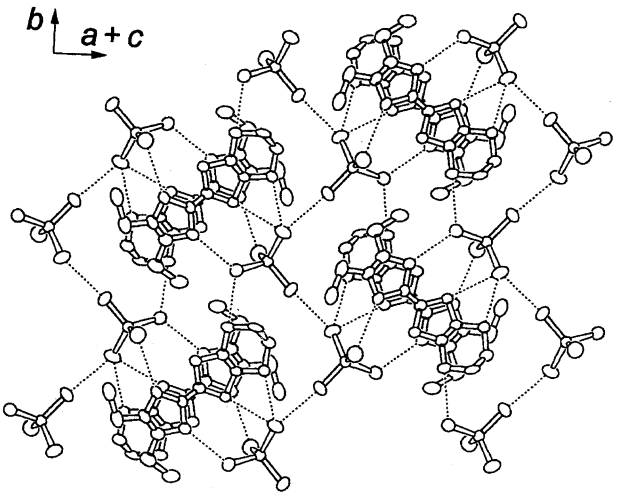

Fig. 14. Structure of C_1TET-TTF·FeBr$_4$ projected on the [10$\bar{1}$] plane. Intermolecular close contacts (see text) are also shown with the dashed lines.

tances (X=Br: 3.608(3), X=Cl: 3.45 Å) are shorter than the sum of van der Waals radii (Br···S: 3.65, Cl···S: 3.55 Å).[62] Therefore the zigzag anion chains are connected with each other by donor dimers, resulting in the formation of a sheet structure, as seen in Fig. 14.

These salts behave as semiconductors ($\sigma_{RT}=2\times10^{-7}$ S cm^{-1}, $E_A=0.43$ eV), as a consequence of the 1 : 1 stoichiometry and the dimerization of donor molecules. Figure 15 shows the magnetic susceptibility of the $FeBr_4$ salt, after the subtraction of the core diamagnetic contribution.[63] The susceptibility obeys the Curie–Weiss law with the antiferromagnetic Weiss temperatures of $\Theta=-6.5$ and -16 K for $FeCl_4$ and $FeBr_4$ salts, respectively. From the Curie constants (X=Cl: 4.41, X=Br: 4.64 emu K mol^{-1}), the observed magnetic moments are assigned to the high-spin FeX_4^- ion ($S=5/2$), consistent with the spin singlet ground state of C_1TET-TTF dimers suggested by the ESR and magnetic susceptibility investigations of the isostructural GaX_4 salt. Although the differences in the X···X and X···S distances between $FeCl_4$ and $FeBr_4$ salts are reasonably explained from the differences in their van der Waals radii, the magnitudes of the exchange interactions are remarkably different. Namely, no distinct magnetic ordering is found for the $FeCl_4$ salt, whereas for the $FeBr_4$ salt the peak of the magnetic susceptibility accompanied by the appearance of anisotropy is observed around 9 K, then an antiferromagnetic transition takes place at $T_N=4.2$ K, below which the spin axis is oriented parallel to the a^*-axis in the ordered state. This difference can be understood as the effect of the polarizability of the anions. The magnetic orbitals of the $FeBr_4^-$ anion are more delocalized to the ligands than those of $FeCl_4^-$ anion, hence the intermolecular exchange interaction of the $FeBr_4$ salt is stronger than the $FeCl_4$ salt. It should also be noted that when the external field is applied parallel to the b-axis (hard axis), a cusp is observed around

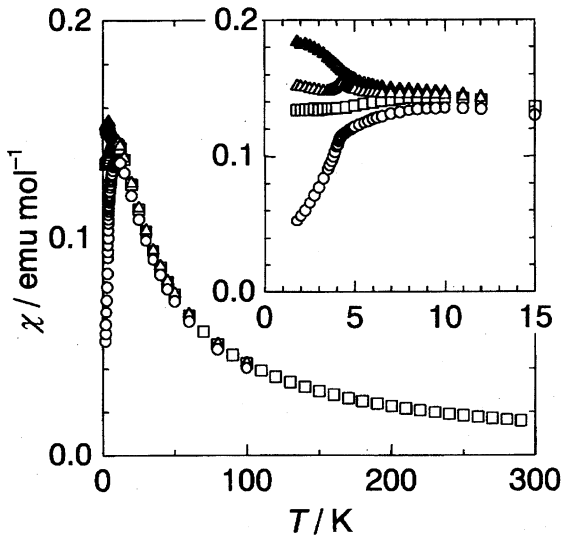

Fig. 15. Temperature dependence of the magnetic susceptibility along the a^*- (○), b- (△), and c-axes (□) in the applied field of $H=1$ T, and along the b-axis (▲) in 3 T for C_1TET-TTF·$FeBr_4$.

T_N, below which a remarkable field dependence in the $\chi(T)$ trace is recognized. On the magnetization curves, besides the presence of a typical spin-flop transition for the a^*-axis at $H_{sf}=2.5$ T, a discontinuous change is observed along the b-axis at the same transition field. Such behavior of the b-axis susceptibility and magnetization is indicative of weak ferromagnetism, whose origin is attributed to the spin canting (//b-axis) due to the Dzyaloshinsky–Moriya asymmetric exchange interaction,[64—66] judging from the absence of any inversion centers between the adjacent anions along the anion chain.

In the spin ordering, the participation of the donor singlet pair is indispensable for the following reasons. Firstly, the ESR spectrum at room temperature of the $FeBr_4$ salt shows only one broad signal ($g=2.03$, $\Delta H\approx100$ mT), and no sharp signals from thermally excited state of the singlet donor, just as seen for the isostructural $GaBr_4$ salt ($g=2.007$, $\Delta H\approx1$ mT), are detected. This reveals the existence of an exchange interaction between the d-electrons on the anion and the π-electrons on the donor units. Secondly, if only the nearest neighbor exchange path along the zigzag anion chain (Fe–Br···Br–Fe) is taken into account, the Néel temperature and the absolute value of the Weiss constant should coincide under the molecular field approximation. In practice, the Néel temperature $T_N=4$ K is suppressed compared with the Weiss constant $\Theta=-16$ K, suggesting the existence of the Fe–Br···(donor)$_2$···Br–Fe exchange path as a second-nearest neighbor antiferromagnetic interaction, which works to frustrate the Fe^{3+} spins, resulting in the lowering of the Néel temperature.

For the next magnetic systems, we discuss FeX_4 (X=Cl, Br) salts of metal-dithiolato complexes, M(dddt)$_2$ (M=Ni, Pd, Pt, Au), from the following viewpoint. These donors have similar molecular structures to that of BEDT-TTF. According to the results of extended Hückel molecular orbital calculations, the HOMOs of M(dddt)$_2$ have the same symmetry as those of BEDT-TTF, with the larger coefficients on the outer sulfur atoms. The larger orbital overlappings between donors and anions are therefore expected.

When nickel is used as a central atom of the donor, the resulting salt has the 3 : 2 stoichiometry,[19,49] which is often observed in the Ni(dddt)$_2$ salts.[67,68] The salts [Ni(dddt)$_2$]$_3$(MX$_4$)$_2$ (M=Fe, Ga; X=Cl, Br) crystallize in monoclinic space group $P2_1/n$ and are isostructural to each other. The unit cell of [Ni(dddt)$_2$]$_3$($FeBr_4$)$_2$ viewed along the c-axis is presented in Fig. 16. Three donor molecules stacked along the a-axis form an A–B–$\bar{A}$ trimer ($\bar{A}$ is related to A by inversion symmetry), with the angle of ca. 25° between the long axes of molecules A and B. While molecule B lies on the inversion center and almost planar, the molecules A and $\bar{A}$ are significantly bent, probably due to the steric effect. The FeX_4^- anions form chains along the c-axis through X···X contacts (distances: Cl: 3.92(2), Br: 3.872(3) Å), then these chains are connected to each other by other X···X contacts along the a-axis (Cl: 4.09(2), Br: 4.070(4) Å) to make two-dimensional corrugated sheets. Close X···S contacts (Br···S: 3.519(3), Cl···S: 3.48(1) Å) are also observed between the

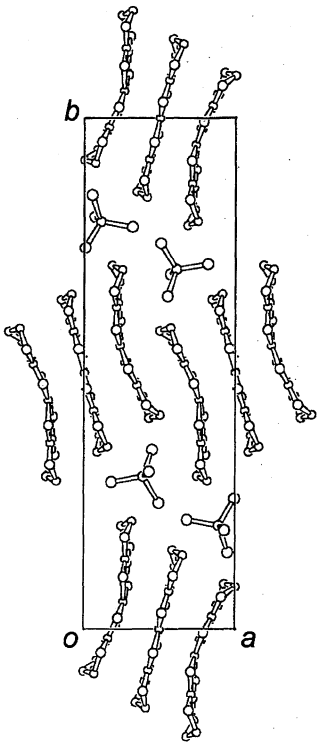

Fig. 16. Crystal structure of $[Ni(dddt)_2]_3(FeBr_4)_2$ viewed along the *b*-axis.

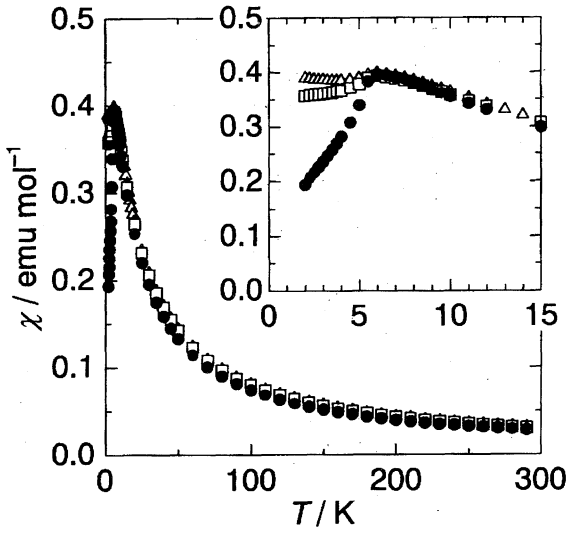

Fig. 17. Temperature dependence of the magnetic susceptibility of $[Ni(dddt)_2]_3(FeBr_4)_2$ along the a^*- (●), *b*- (△), and *c*-axis (□) in the applied field of H=1 T.

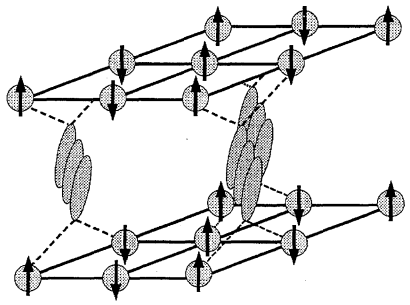

Fig. 18. Schematic drawing of the magnetic structure of $[Ni(dddt)_2]_3(FeBr_4)_2$. The arrows with shaded circles denote magnetic Fe^{3+} sites, while bunches of ellipsoids give donor trimers. Contacts between counter anions are depicted with solid lines, and contacts between donors and anions are drawn with dashed lines.

six-membered rings of the donors and the anion sheets. Compared to the sum of the corresponding van der Waals radii,[62] the intermolecular contacts between halogen atoms are relatively weak, while the donor-anion contacts are significantly strong; hence the π–*d* interactions through the latter contacts are readily expected.

These salts show semiconductive behavior with similar room temperature conductivities and activation energies, regardless of the counter anions (ρ_{RT}=3 Ω cm, E_A=0.13 eV). In addition, the ESR investigation gives no distinguishable signal for the isostructural $GaBr_4$ salt, indicating the π-electrons on the donor molecules have singlet ground state, which agrees with the energy band structure calculation showing the energy gap E_g=0.06 eV between the conduction and valence bands. The magnetic susceptibility obeys the Curie–Weiss law with Weiss temperatures Θ=−4.7 K (X=Cl) and −12.5 K (X=Br), as shown in Fig. 17. The absence of the short-range order peak in the susceptibility curve suggests three-dimensionality in the superexchange path network. For both salts, antiferromagnetic transitions are observed at T_N=2.5 and 6.0 K for X=Cl and Br, respectively, below which the easy spin axis is oriented along the *c*-axis, as shown in the inset of Fig. 17. Consequently, the three-dimensional feature in the magnetism proves that, besides the intralayer exchange interaction between the FeX_4^- anion through the X···X contacts, the superexchange interlayer interaction through Fe–X···$[Ni(dddt)_2]_3$···X–Fe should play an essential role in the realization of the magnetic long range order. Figure 18 schematically illustrates a possible magnetic structure in the ordered state. Since one donor trimer working to mediate antiferromagnetic superexchange paths contacts to four neighboring $FeBr_4^-$ anions with an antiparallel spin alignment on the $FeBr_4^-$ anion layer, the competition between antiferromagnetic interactions makes the Néel temperature (6.0 K for X=Br) suppressed compared to the Weiss constant (Θ=−12.5 K for X=Br).

If the dithiolato complexes of Pd, Pt or Au are used as donor molecules, the salts with 2 : 1 stoichiometry are obtained.[49] Judging from the cell constants and the systematic absence of their Bragg reflections, all salts belonging to this group are isostructural to each other, regardless of the metal atoms of the donor (Pd, Pt, Au), the anions (Fe, Ga), and the ligand atoms of the anion (Cl, Br). Figure 19 shows the unit cell of $[Au(dddt)_2]_2GaBr_4$ viewed along the *b*-axis. Two donor molecules form a dimer coupled by a metal–metal contact and, as a result, the molecules are bent from the planarity. The strength of the contact depends on the central metal ($[Pd(dddt)_2]_2FeCl_4$: 3.019(1), $[Pt(dddt)_2]_2FeCl_4$: 2.966(1),[69] $[Au(dddt)_2]_2GaBr_4$: 3.430(2) Å). The donor dimers are then stacked along the $a+b$ direction to form

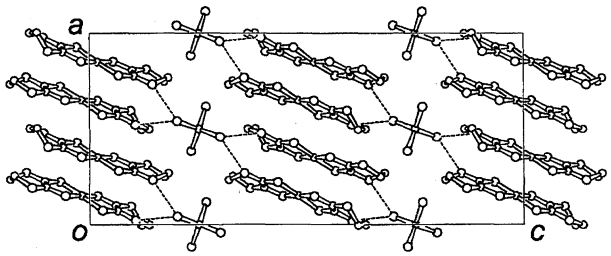

Fig. 19. Crystal structure of $[Au(dddt)_2]_2FeBr_4$ viewed along the *b*-axis. Close intermolecular contacts between donors and anions are shown with dashed lines.

the donor columns, between which there are a number of S···S contacts closer than twice the van der Waals radius of sulfur (3.70 Å).[62] The nearest intermolecular halogen–halogen distance is too large (4.694(8) Å for $[Au(dddt)_2]_2GaBr_4$) for the localized Fe^{3+} spins on the anions to interact directly with each other. On the other hand, there are two close halogen···sulfur contacts between the donor and the anion, as indicated with the dashed line in Fig. 19. Since the distance of the closest one (3.674(9) Å for $[Au(dddt)_2]_2GaBr_4$) is close to the sum of van der Waals radii (Br···S: 3.65 Å),[62] the counter anions are connected through these contacts toward the donor dimer.

These salts show semiconductive behavior with the room temperature conductivity of σ_{RT}=0.1 S cm^{-1} and the activation energy of E_A=800 K, regardless of the central metals of the donor molecules and counter anions. The band structure calculation, however, predicts the metallic behavior with the presence of two Fermi surfaces. One possible explanation of this discrepancy is the emergence of the Peierls state, as a consequence of the one-dimensional character of the Fermi surfaces. Another possibility is the effect of the large on-site Coulomb repulsion coming from the dimerization of the donor molecules, which derives the localization of the conduction electrons within the donor columns. Since the magnetic susceptibility of $[Au(dddt)_2]_2GaBr_4$ shows Curie-like behavior, the second explanation is more plausible.

The magnetic susceptibility of $[M(dddt)_2]_2FeCl_4$ (M=Pt, Au) obeys the Curie law regardless of the center metal atoms, hence there is an absence of appreciable interaction between the magnetic anions in these materials. On the other hand, the susceptibility of $[M(dddt)_2]FeBr_4$ shows the Curie–Weiss behavior (M=Pt: Θ=−5.9 K, M=Au: Θ=−4.6 K) with a maximum at 4.5 K for Pt and 2.8 K for Au complex, as shown in Fig. 20. For the $Pt(dddt)_2$ salt, an antiferromagnetic transition takes place at T_N=4.5 K, below which the spin easy axis is oriented along the *a*-axis. Since there is no direct contact between the anions, the exchange interaction between two Fe^{3+} S=5/2 spins should be mediated by one S=1/2 spin localized on the dimer unit $[M(dddt)_2]_2$ through the path of Fe–Br···$[M(dddt)_2]_2$···Br–Fe. In these salts the difference in magnetic behavior between the $FeCl_4$ and $FeBr_4$ salts can be understood again as the result of high polarizability of $FeBr_4^-$ anions. Furthermore, the difference between the Pt-$(dddt)_2$ and $Au(dddt)_2$ salts can be explained qualitatively from the result of the extended Hückel molecular orbital

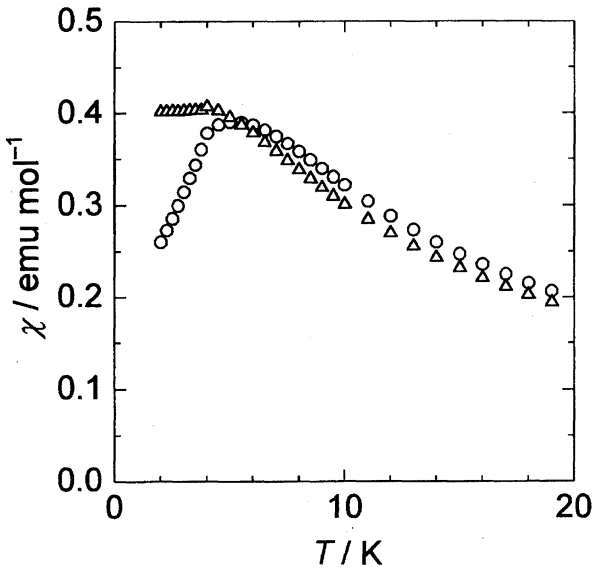

Fig. 20. Temperature dependence of the magnetic susceptibility of $[Pt(dddt)_2]_2FeBr_4$ along the *a*- (○) and *b*-axis (△) in the applied field of H=1 T.

calculations. The magnetic orbitals of the donors in these two salts correspond to the HOMO of the neutral $Pt(dddt)_2$ (b_{3u}) and the SOMO of $Au(dddt)_2$ (b_{1g}), respectively, as presented in Fig. 21. Only for the b_{1g} orbital the contribution of the metal *d*-orbitals exists and the donation of π-electrons from the ligand to the metal occurs; hence the electron density on the outer sulfur atoms of the b_{1g} orbital is smaller than that of the b_{3u} orbital. Therefore the unpaired electron spin of the $Pt(dddt)_2$ dimer is more delocalized to the outer sulfur atom than the $Au(dddt)_2$ dimer, which makes the transfer integral between $Pt(dddt)_2$ and the anion larger than that of the $Au(dddt)_2$ case.

2-2. System with the Coexistence of Magnetism and Electron Transport. $(BEDT\text{-}TTF)_3CuBr_4$ belongs to a novel class of organic cation radical salts including a magnetic counter anion.[46,47,52,53,70] It has interesting phase transitions at T_c=59 K and T_N=7.65 K with drastic changes in magnetic properties related to the coexistence of the π–*d* interaction.

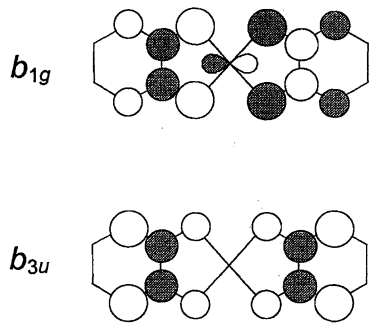

Fig. 21. Schematic drawing of the frontier orbitals of $M(dddt)_2$ molecules. For M=Pt, b_{3u} and b_{1g} orbitals correspond to HOMO and LUMO, respectively, whereas for M=Au, they correspond to NHOMO and SOMO, respectively.

This salt consists of alternating stacking of BEDT-TTF π-electron sheets and Cu^{2+} magnetic counter anion sheets. Figure 22 shows the crystal structure at room temperature projected along the central C=C bonds of BEDT-TTF molecules.[70—73] The anion layer forms a quasi square lattice with the Cu^{2+} magnetic moments. The donor layer has two independent BEDT-TTF molecules; that is, one A molecule in the neutral state and two B molecules with a +1 charge in a formula unit $(BEDT\text{-}TTF)_3CuBr_4$. In the anion layer, the shortest anion–anion (Br···Br) distance is 4.190(1) Å, which is considerably larger than the sum of corresponding van der Waals radii 3.70 Å. Meanwhile, there are several close donor–anion (Br···S) contacts with the distances of 3.699(3), 3.752(3), 3.774(3), and 3.821(3) Å for the external S atoms of BEDT-TTF molecules having the small density of π-electrons in the HOMO level, in comparison with the sum of corresponding van der Waals radii 3.65 Å.[62] Thus, in the present compound, the donor–anion interaction is suggested to dominate the magnetic interaction over the direct anion–anion interaction from the consideration of the intermolecular atomic distances.

Figure 23a shows the temperature dependence of the spin susceptibility in the applied field of H=0.4T parallel to the b-axis. The magnetic susceptibility shows the Curie–Weiss behavior above T_c=59 K. Since the ESR signals of the BEDT-TTF cation radical and the $CuBr_4^{2-}$ anion coalesce, there is strong exchange interaction between the π-electrons on the BEDT-TTF molecules and the localized Cu d-electrons. We can therefore analyze the susceptibility using a single Curie–Weiss equation above T_c. The analysis gives the antiferromagnetic Weiss temperature Θ=−100 K and the spin density N≈3 with S=1/2 in a formula unit. Taking into account that BEDT-TTF B molecules are in the cation radical state with a +1 charge, the observed spins are assigned to two BEDT-TTF B molecules and one $CuBr_4^{2-}$ ion having magnetic moments with S=1/2. At T_c=59 K, the susceptibility drops discontinuously by 40% from the value just above T_c without the appearance of any anisotropy between the a^*, b, and c-axes. The decrease of the spin density at T_c is interpreted as the disappearance of the localized π-electron spins on BEDT-TTF B cation radicals, judging from the absence of the contribution of the donor spin to the ESR spectra and the theoretical fitting of the static susceptibility (N≈1). As a consequence, only Cu^{2+} spins contribute to the magnetic behavior below T_c. Below T_c, the susceptibility has a hump around 28 K due to the magnetic short range order in the low-dimensional antiferromagnet, and then it shows a small peak of an antiferromagnetic transition at T_N=7.65 K. The Cu^{2+} sites form a distorted square magnetic lattice; thus, taking into account the isotropic nature of Cu^{2+} spins, the susceptibility with the hump can be fitted to the theory of the two-dimensional square lattice Heisenberg antiferromagnet

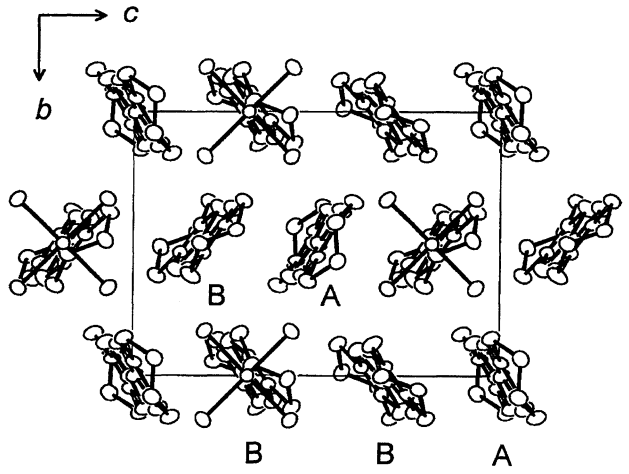

Fig. 22. Structure of $(BEDT\text{-}TTF)_3CuBr_4$ at room temperature projected along the central C=C bonds in the BEDT-TTF molecules. The Cu^{2+} ions form a two-dimensional quasi square lattice. A and B denote two independent BEDT-TTF molecules, where A is in the neutral state and B has a +1 charge.

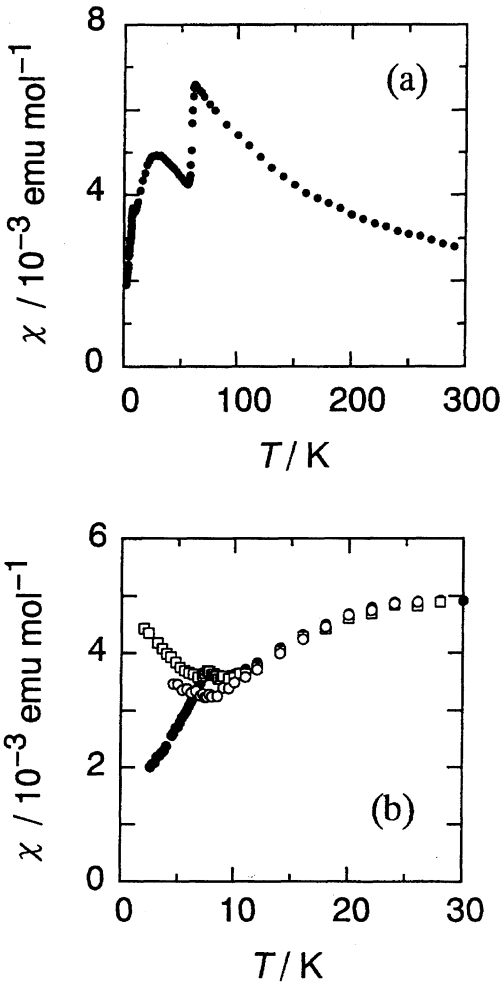

Fig. 23. a) Temperature dependence of magnetic susceptibility in the field of H=0.4 T applied parallel to the b-axis. The mole unit corresponds to the formula unit of $(BEDT\text{-}TTF)_3CuBr_4$. b) Temperature dependence of magnetic susceptibility in the applied field parallel to the a^* (○), b (●), and c (□)-axes in the low temperature region below 30 K. The antiferromagnetic transition temperature is estimated at T_N=7.65 K from the appearance of the anisotropic behavior.

model,[13] which gives an estimate of the intralayer exchange interaction of $J_{d-d}=-15.7$ K between Cu^{2+} spins. Figure 23b shows the detailed temperature dependence of magnetic susceptibility below 30 K in the field applied parallel to the a^*, b, and c-axes. Below T_N, the susceptibility for the b-axis drops, while it is elevated for the a^* and c-axes with decreasing the temperature, which indicates that the magnetic easy axis lies almost on the b-axis. The existence of the antiferromagnetic transition evidences the important role of the interlayer interaction between the Cu^{2+} layers, because no long range order exists at a finite temperature in pure two-dimensional Heisenberg antiferromagnets.[47]

The temperature-pressure phase diagram related to the electronic and magnetic properties is summarized in Fig. 24, based on the results of the resistivity and ^{1}H NMR under pressure.[70,75,76] In the phase diagram, the high temperature insulator phase I(I) with the localized magnetic moments of BEDT-TTF B molecules borders the low temperature insulator phase I(II) where the magnetic moments disappear. In the high temperature range above the boundary of insulator phase I(II), the increase of pressure changes the phase from the insulator I(I) to the metallic M(I) around 7 kbar, and finally stabilizes the metallic M(II) phase above 13 kbar. It should be noted that the magnetic susceptibility in the phase I(I) becomes reduced in the vicinity of the phase boundary to M(I). The application of pressure makes the Néel temperature for the Cu^{2+} magnetic lattice increase linearly and approach to 15 K around 20 kbar.

First, we discuss the electrical and magnetic properties in the insulator I(I) phase above $T_c=59$ K under ambient pressure. The presence of localized spins on BEDT-TTF B molecules indicates that the electronic and magnetic states of the BEDT-TTF layer in the high temperature I(I) phase is characterized as a Mott insulator where the on-site Coulomb repulsion overwhelms the transfer integral. However, the composition of the present compound gives 2/3 filled band structure, if we neglect the difference between the A and B sites. This is not favorable for an ordinary Mott insulator because Mott insulators require the half-filled band structure within the one electron picture, where the on-site Coulomb repulsion works most effectively. The experimental finding proves the presence of the charge separation between +1 (B) and neutral (A),[77,78] which is thought to give the HOMO level splitting into upper four-fold and lower two-fold sublevels.[79] Therefore, the upper band has the intrinsic half-filled band structure, which causes the Mott insulating state. It is worth noting the presence of strong antiferromagnetic interaction between the localized π-electrons on BEDT-TTF molecules and the localized d electrons on $CuBr_4^{2-}$ ions, as evidenced by the large negative Weiss temperature $\Theta=-100$ K in addition to the single Lorentzian ESR lineshape. As a consequence, this compound is characterized as the "π–d composite magnet" in the I(I) phase with the strong exchange interaction between the BEDT-TTF π-spins and Cu^{2+} d-spins.

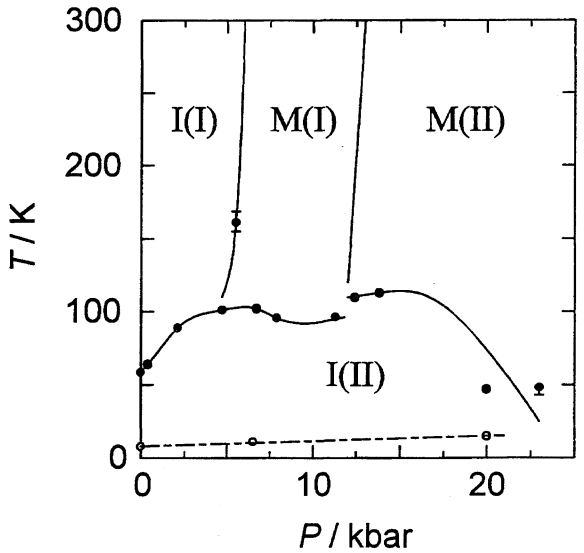

Fig. 24. Temperature–pressure phase diagram.[46,73,76] I(I) and I(II) denote the insulator phases, while M(I) and M(II) do the metallic phases. The dash-dotted line indicates the pressure dependence of the antiferromagnetic transition for the Cu^{2+} magnetic lattice obtained by ^{1}H NMR.

The changes in the pressure and temperature bring about a large variety of phase changes, as summarized in Fig. 24. In this connection, the behavior at high pressures toward metallic states gives important information related to the competition between the transfer integral and the on-site Coulomb interaction in the Mott–Hubbard system. That is, the application of pressure enhances the transfer integral, while it dose not change the on-site Coulomb interaction effectively. As a matter of fact, the remarkable decrease in the resistivity[70] proves the increase of the transfer integrals in comparison with the small change of the on-site Coulomb interaction, resulting in the appearance of the metallic phases. Moreover, in the high pressure region, the application of pressure enhances the donor–anion contacts, which brings about the increase of the magnetic interaction between the conduction π-electrons and the localized d-electrons. In this sense, the conduction π-electrons are scattered by the localized d-electrons through the exchange interaction, which reminds us of the s–d interaction in ordinary magnetic metals of inorganic transition metal compounds. Consequently, in the high pressure metallic regions M(I) and M(II), this compound is considered to behave as the "π–d Kondo system", which is expected to give a molecule-based metal magnet. The feature of the magnetic ordering of the Cu^{2+} lattice gives interesting behavior in this connection. According to the result in Fig. 24, the application of pressure raises the Néel temperature for the Cu^{2+} magnetic lattice, while it lowers the phase boundary between the metallic M(II) and the insulating I(II) above 15 kbar, resulting in the stabilization of the metallic state. The Néel temperature tends to cross the metal-insulator boundary around 25 kbar. Therefore, we can expect interesting magnetic features realized as a molecule-based metal magnet in the high pressure range.

In the case of the phase transition from I(I) to I(II) at T_c, the structural deformation plays the key role that drives the

change in the electronic structure. As mentioned above, the Mott insulating state I(I) is closely related to the charge disproportionation between BEDT-TTF A and B molecules. In the meantime, the charge distribution becomes almost uniform below T_c according to the X-ray structure analysis.[77,78] The disappearance of the charge separation implies that the I(II) phase below T_c is not characterized as a Mott insulating state, which is in good agreement with the experimental findings that the magnetic moments on BEDT-TTF molecules disappear at T_c. Moreover, the electrical resistivity shows the semiconductive behavior with a small activation energy below T_c. These results suggest that the electronic structure in the I(I) phase can be described by a band insulator with a narrow band gap. As a consequence, the structural transition at T_c with the disappearance of the magnetic moments on BEDT-TTF B molecules is thought to be the transition from the Mott insulator to the band insulator.

Now, we discuss the origin of the strong π–d interaction. The exchange interaction energy of $J_{d-d}=-15.7$ K between the Cu^{2+} sites is significantly large in spite of the long interatomic distances Cu···Cu (8.724(1) Å) and Br···Br (4.190(1) Å) between the nearest neighbor $CuBr_4^{2-}$ anions in the Cu^{2+} magnetic layer. In order to clarify the reason for the large exchange interaction, we calculate the electronic structure of $CuBr_4^{2-}$ using DV-$X\alpha$ method. The result suggests that, in the HOMO wave function, the Cu 3d electron is delocalized to the peripheral ligand region of the $CuBr_4^{2-}$ anion through the hybridization of the Cu-3d and Br-4p orbitals.[70] This is a specific feature in the electronic structure of $CuBr_4^{2-}$ different from other transition metal halide anions, that is related to the trend in the strengths of exchange interactions in the family of 3d-transition metal halides[58] as mentioned in Section 2-1. Therefore, the extended nature of the localized d-electrons is thought to cause partly the large interlayer interaction, in spite of the long inter-anion atomic distances in the magnetic layer. Moreover, the large Weiss temperature and the Lorentzian line shape of ESR above T_c indicates the presence of the strong antiferromagnetic exchange interaction between the localized π-spins on BEDT-TTF molecules and the Cu^{2+} d-spins. Taking into account that the van der Waals distance is 3.8 Å for the Br···S atomic contact,[62] we find that the shortest distance of 3.699(3) Å between the Br atom of $CuBr_4^{2-}$ and the external S atom of BEDT-TTF B molecule is short enough to realize the orbital overlap. Thus, the delocalized d-electrons, which are the origin of magnetic moments of the Cu^{2+} ions, can easily interact with the π-electrons delocalized on the BEDT-TTF donors. Therefore, the cooperation of the novel electronic structure of $CuBr_4^{2-}$ and the close donor-anion contacts causes the strong exchange interaction between the donor π-electrons and the localized d-electrons.

Finally, we discuss the mechanism of the antiferromagnetic ordering below T_N, which takes place on the Cu^{2+} magnetic lattice. According to the mean field theory, the perpendicular susceptibility at $T=0$ is given by $\chi_\perp(0)=Ng_{Cu}\mu_B/4z_{Cu}J_{d-d}$, where N, $z_{Cu}=4$ and g_{Cu} are the number of Cu^{2+} spins and the number of nearest neighbors for the Cu^{2+} magnetic square lattice, and the g-value of the Cu^{2+} spin, respectively. Meanwhile, in the low-dimensional Heisenberg antiferromagnet, the quantum spin fluctuation causes the spin contraction that lowers the perpendicular susceptibility below T_N in comparison with that expected by the mean field theory. From the equation of the spin wave theory,[80] the perpendicular susceptibility at $T=0$ is estimated at $\chi_\perp(0)=3.07\times10^{-3}$ emu mol^{-1}, while the observed value of the perpendicular susceptibility for the c-axis is extrapolated to $\chi_\perp(0)=4.8\times10^{-3}$ emu mol^{-1} at $T=0$ K, which is 56% as large as the predicted susceptibility value. Since the enhancement in the dimensionality reduces the zero-point spin contraction,[74] the difference between the predicted and the observed values can be ascribed to the presence of the interlayer interaction. Nevertheless, the interlayer interaction is not realized through the ordinary superexchange path of σ-bonds because the interlayer distance 17 Å of $CuBr_4^{2-}$ ions is too long. Consequently, it is suggested that the interlayer interaction between Cu^{2+} spins is mediated by the superexchange path of the π-orbitals on BEDT-TTF molecules. This is supported by the result that the magnetic heat capacity obeys the cubic temperature dependence, which evidences the presence of the three-dimensional nature in the antiferromagnetically ordered state.[80,81] In conclusion, the antiferromagnetic ordering in the Cu^{2+} magnetic lattice is associated importantly with the interlayer interaction through the π-orbitals on BEDT-TTF molecules.

3. Conclusion

TTF-type organic donors form charge transfer complexes with various kinds of anions, which give a large variety of low dimensional electronic systems among insulators, semiconductors, metals and superconductors consisting of π-electrons. In these materials, the relative ratio of transfer integral to on-site Coulomb repulsion plays an important role in their transport properties; that is, the increase in the transfer integral varies the materials from insulating state to metallic one, whereas the decrease in the transfer integrals, which emphasizes the role of the on-site Coulomb interaction, brings about the localization of electrons, leading to the formation of insulating states. Form the aspect of magnetism, the localized π-electrons generated in the insulating regime give rise to low-dimensional magnetic systems based on their localized magnetic moments. The introduction of magnetic anions having d-electrons into the organic charge transfer complexes also generates magnetic systems, where the π-electrons, if the π-electronic system has delocalized features in the metallic regime with large transfer integrals, can give organic analogues of metal magnets through the π–d interactions. In the meantime, localized magnetic d-electrons embedded in insulating complexes are expected to interact with each other through the superexchange paths mediated by organic π-electrons, if there are inter-molecular interactions between organic molecules and counter ions with magnetic d-electrons.

We have developed magnetic systems based on TTF-type organic donors. In the present accounts, we present two

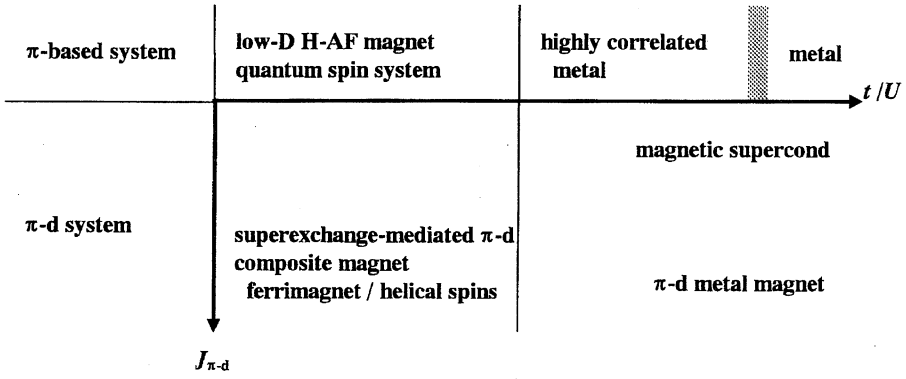

Fig. 25. Overview of magnetism appearing in the organic charge transfer complexes through the interplay among the transfer integral t, the on-site Coulomb interaction U and the π–d interaction $J_{\pi-d}$. Low-dimensional Heisenberg antiferromagnet is abbreviated as "low-D H-AF magnet", while "magnetic supercond" denotes magnetic superconductor.

kinds of magnetic systems; π-electron-based low-dimensional molecular magnets and magnets with π–d interactions. In the class of π-electron-based low-dimensional magnets, β'-(BEDT-TTF)$_2$X (X=ICl_2, $AuCl_2$) give features of two-dimensional square lattice Heisenberg antiferromagnetic systems, while (C_1TET-TTF)$_2$Br is described in terms of two-dimensional distorted triangular lattice Heisenberg antiferromagnetic system, where its quantum spin characteristics induce a large spin frustration effect. (BEDT-TTF)$_2$Br·CH_2(OH)CH_2OH is in metallic state around room temperature with the presence of localized magnetic moments, revealing the feature of a highly correlated metallic system. The variety of phase transition behavior related to magnetism and electron transport gives attractive issues of spin-charge separation in the highly correlated electron systems. C_1TET-TTF·$FeBr_4$, [Ni(dddt)$_2$]$_3$($FeBr_4$)$_2$, and [M(dddt)$_2$]$_2$$FeBr_4$ (M=Pd, Pt, Au) undergo three-dimensional magnetic long range ordering through the π-electron-mediated superexchange interaction. In (BEDT-TTF)$_3$$CuBr_4$, the cooperation of d-localized magnetic moments and π-conduction carriers gives the novel correlation between magnetism and electron transport through the π–d interaction.

As mentioned above, organic complex-based molecular magnets are found to be good targets for the current topics on the development of molecular magnetism, molecular design for functional materials and the physics of highly correlated electron systems. As a strategic overview, Fig. 25 summarizes a diversity of magnetism emerging in the charge transfer complexes through the interplay among the transfer integral, the on-site Coulomb interaction and the π–d interaction. The molecular design on the π-electron-based low-dimensional magnetic systems will provide a novel class of quantum spin systems that have never been known in ordinary inorganic magnetic systems. π-electron based complexes are an important mine of highly correlated electron materials, with which physicists can try to figure out the problems on the Mott–Hubbard systems. In connection with the π–d systems, superexchange-mediated π–d composites in the insulating regime are expected to provide ferrimagnets, weak ferromagnets or helical magnets, while metallic π–d systems happen to become organic magnetic superconductors[55] by chance unless the π–d interaction is strong enough to bring about the pair breaking against the superconducting state. Moreover, in addition to (BEDT-TTF)$_3$$CuBr_4$, organic complexes being recently found (DMe-DCNQI)$_2$Cu[82,83] and λ-(BEDT-TSF)$_2$$FeCl_4$[57,84] have been currently targeted as prototypical systems of the π–d interaction for their peculiar correlation between magnetism and electron transport. The π–d interaction in metallic complexes will open a new frontier field of organic metal magnets with strong magnetic interaction.

The present authors would like to express their sincere thanks to N. Yoneyama, M. Enomoto, K. Yamaguchi, T. Umeyama, M. Enomoto, K. Suzuki in their group, who contributed to the studies of the organic complex-based magnets introduced in these accounts. They also thank Prof. N. Kojima of the University of Tokyo and Prof. H. Tanaka of Tokyo Institute of Technology for fruitful discussions. This work is partly supported by the Grant-in-Aid for Scientific Research on Priority Area "Novel Electronic States in Molecular Conductors" (Area No. 253/07232216) from the Ministry of Education, Science, Sport and Culture.

References

1) H. Aakamatsu, H. Inokuchi, and Y. Matsunaga, *Nature*, **173**, 168 (1954).

2) M. Tamura, Y. Nakazawa, D. Shiomi, K. Nozawa, Y. Hosokoshi, M. Ishikawa, M. Takahashi, and M. Kinoshita, *Chem. Phys. Lett.*, **186**, 401 (1991).

3) J. M. Williams, J. R. Ferraro, R. J. Thorn, K. D. Carlson, U. Geiser, H. H. Wang, A. M. Kini, and M.-H. Whangbo, "Organic Superconductors (Including Fullerenes); Synthesis, Structure, Properties, and Theory," Prentice Hall, Englewood Cliffs, New Jersey (1992).

4) J.-P. Farges, "Organic Conductors; Fundamentals and Applications," Marcel- Dekker Inc., New York (1994).

5) N. Yoneyama, A. Miyazaki, T. Enoki, and G. Saito, *Synth. Met.*, **86**, 2029 (1997).

6) J. Yamaura, A. Miyazaki, T. Enoki, and G. Saito, *Phys. Rev.*, **B55**, 3649 (1997).

7) T. J. Emge, H. H. Wang, P. C. W. Leung, P. R. Rust, J.

D. Cook, P. L. Jackson, K. D. Carlson, J. M. Williams, M.-H. Whangbo, E. L. Venturini, J. E. Shriber, L. J. Azevedo, and J. R. Ferraro, *J. Am. Chem. Soc.*, **108**, 695 (1986).

8) H. Kobayashi, R. Kato, A. Kobayashi, G. Saito, M. Tokumoto, H. Anzai, and T. Ishiguro, *Chem. Lett.*, **1986**, 89.

9) L. I. Buravov, A. V. Zvarykina, A. A. Ignat'ev, A. I. Kotov, V. N. Laukhin, M. K. Makova, V. A. Merzhanov, L. P. Rozenberg, P. P. Shibaeva, and E. B. Yagubskii, *Bull. Acad. Sci. USSR*, **1989**, 1815.

10) T. J. Emge, H. H. Wang, M. K. Bowman, C. M. Pipan, K. D. Carlson, M. A. Beno, L. N. Hall, B. A. Anderson, J. M. Williams, and M.-H. Whangbo, *J. Am. Chem. Soc.*, **109**, 2016 (1987).

11) T. Mori and H. Inokuchi, *Solid State Commun.*, **62**, 525 (1987).

12) T. Mori, A. Kobayashi, Y. Sasaki, H. Kobayashi, G. Saito, and H. Inokuchi, *Bull. Chem. Soc. Jpn.*, **57**, 627 (1984).

13) M. E. Lines, *J. Phys. Chem. Solids*, **31**, 101 (1971).

14) T. Oguchi, *Phys. Rev.*, **133**, A1098 (1964).

15) C. Coulon, R. Laversanne, J. Amiell, and P. Delhaes, *J. Phys. C*, **19**, L753 (1986).

16) W. A. Harrison, "Electronic Structure and The Properties of Solids; The Physics of The Chemical Bond," Dover, New York (1980).

17) M. A. Beno, M. A. Firestone, P. C. W. Leung, L. M. Sowa, H. H. Wang, J. M. Williams, and M.-H. Whangbo, *Solid State Commun.*, **57**, 735 (1993).

18) S. D. Obertelli, R. H. Friend, D. R. Talham, M. Kurmoo, and P. Day, *J. Phys.: Condens. Matter*, **1**, 5671 (1989).

19) T. Enoki, M. Enomoto, M. Enomoto, K. Yamaguchi, N. Yoneyama, J. Yamaura, A. Miyazaki, and G. Saito, *Mol. Cryst. Liq. Cryst.*, **285**, 19 (1996).

20) M. Tokumoto, H. Anzai, and T. Ishiguro, *Synth. Met.*, **19**, 215 (1987).

21) H. Kobayashi, R. Kato, A. Kobayashi, Y. Nishio, K. Kajita, and W. Sasaki, *Chem. Lett.*, **1986**, 833.

22) The effective on-site Coulomb interaction U_{eff} defined as the on-site Coulomb energy on a dimer unit is given by $U_{\mathrm{eff}} = (U - \sqrt{U^2 + 4t_{\mathrm{intra}}{}^2})/2 + 2|t_{\mathrm{intra}}| \approx 2|t_{\mathrm{intra}}| (U \gg |t_{\mathrm{intra}}|)$, where U is the on-site Coulomb energy of the individual donor and t_{intra} is the intra-dimer transfer integral.

23) H. Kawamura and S. Miyashita, *J. Phys. Soc. Jpn.*, **53**, 9 (1984).

24) P. W. Anderson, *Mat. Res. Bull.*, **8**, 153 (1973).

25) M. Tokumoto, H. Anzai, T. Ishiguro, G. Saito, H. Kobayashi, R. Kato, and A. Kobayashi, *Synth. Met.*, **19**, 215 (1987).

26) T. Komatsu, H. Sato, T. Nakamura, N. Matsukawa, H. Yamochi, G. Saito, M. Kusunoki, K. Sakaguchi, and S. Kagoshima, *Bull. Chem. Soc. Jpn.*, **68**, 2223 (1995).

27) H. Kawamura and S. Miyashita, *J. Phys. Soc. Jpn.*, **53**, 4138 (1984).

28) Y. Ajiro, H. Kikuchi, S. Sugiyama, T. Nakashima, S. Shamoto, N. Nakayama, M. Kiyama, N. Yamamoto, and Y. Oka, *J. Phys. Soc. Jpn.*, **57**, 2268 (1988).

29) T. Mori and H. Inokuchi, *Chem. Lett.*, **1987**, 1657.

30) M. J. Rosseinsky, M. Kurmoo, D. R. Talham, P. Day, D. Chasseau, and D. Watkin, *J. Chem. Soc., Chem. Commun.*, **1988**, 88.

31) R. P. Shibaeva, R. M. Lobkovskaya, L. P. Rozenberg, L. I. Buravov, A. A. Ignatiev, N. D. Kushch, E. E. Laukhina, M. K. Makova, E. B. Yagubskii, and A. V. Zvarykina, *Synth. Met.*, **27**, A189 (1988).

32) H. Urayama, G. Saito, A. Kawamoto, and J. Tanaka, *Chem. Lett.*, **1987**, 1753.

33) N. P. Karpova, S. V. Konovalikhin, O. A. Dyachenko, R. N. Lyubovskaya, and E. I. Zhilyaeva, *Acta Crystallogr., Sect. C*, **C48**, 62 (1992).

34) A. Miyazaki, K. Yamaguchi, T. Enoki, and G. Saito, *Synth. Met.*, **86**, 2033 (1997).

35) T. Enoki, K. Imaeda, M. Kobayashi, H. Inokuchi, and G. Saito, *Phys. Rev.*, **B33**, 1553 (1986).

36) J. C. Bonner and M. E. Fisher, *Phys. Rev.*, **135**, A640 (1964).

37) J. W. Hall, W. E. Marsh, R. R. Weller, and W. Hatfield, *Inorg. Chem.*, **20**, 1033 (1981).

38) A. Miyazaki, T. Enoki, H. Uekusa, Y. Ohashi, and G. Saito, *Phys. Rev.*, **B55**, 6847 (1997).

39) K. Yamaguchi, A. Miyazaki, T. Enoki, and G. Saito, private communication.

40) R. E. Dietz, F. R. Merritt, R. Dingle, D. Hone, B. G. Silbernagel, and P. M. Richard, *Phys. Rev. Lett.*, **26**, 1186 (1971).

41) M. Date, H. Yamazaki, M. Motokawa, and S. Tazawa, *Prog. Theor. Phys., Suppl.*, **S46**, 194 (1970).

42) M. Tanaka, A. Kawamoto, J. Tanaka, M. Sano, T. Enoki, and H. Inokuchi, *Bull. Chem. Soc. Jpn.*, **60**, 2531 (1987).

43) M. Tanaka, A. Kawamoto, J. Tanaka, M. Sano, T. Enoki, and H. Inokuchi, *Jpn. J. Appl. Phys.*, **26**, 893 (1987).

44) T. Enoki, I. Tomomatsu, Y. Nakano, K. Suzuki, and G. Saito, "The Physics and Chemistry of Organic Superconductors," ed by G. Saito and S. Kagoshima, Springer Verlag, Berlin (1990), p. 294.

45) P. Wang, T. Mori, S. Bandow, Y. Maruyama, X. Wang, B. Chen, D. Zhu, K. Tsujikawa, K. Suzuki, and T. Enoki, *Synth. Met.*, **49**, 253 (1992).

46) K. Suzuki, J. Yamaura, N. Sugiyasu, T. Enoki, and G. Saito, *Synth. Met.*, **56**, 1741 (1993).

47) T. Enoki, J. Yamaura, N. Sugiyasu, K. Suzuki, and G. Saito, *Mol. Cryst. Liq. Cryst.*, **233**, 325 (1993).

48) T. Enoki, J. Yamaura, N. Sugiyasu, Y. Nakano, and K. Suzuki, "New Functionality Materials," ed by T. Turuta, M. Doyama, and M. Seno, Elsevier Science Publisher B. V., Vol. C, "Synthetic Process and Control of Functionality Materials," p. 509 (1993).

49) A. Miyazaki, M. Enomoto, M. Enomoto, T. Enoki, and G. Saito, *Mol. Cryst. Liq. Cryst.*, (1997), in press.

50) T. Mallah, C. Hollis, S. Bott, M. Kurmoo, P. Day, M. Allan, and R. H. Friend, *J. Chem. Soc., Dalton Trans.*, **1990**, 859.

51) P. Day, M. Kurmoo, T. Mallah, I. R. Marsden, R. H. Friend, F. L. Pratt, W. Hayes, D. Chasseau, J. Gaultier, G. Bravic, and L. Ducasse, *J. Am. Chem. Soc.*, **114**, 10722 (1992).

52) M. Kurmoo, D. Kanazawa, P. Day, I. R. Marsden, M. Allan, and R. H. Friend, *Synth. Met.*, **55-57**, 2347 (1993).

53) M. Kurmoo, P.Day, M. Allan, and R. H. Friend, *Mol. Cryst. Liq. Cryst.*, **234**, 199 (1993).

54) C. J. Gomez-Garcia, L. Ouahab, S. Triki, E. Coronado, and P. Delhaès, *Angew. Chem., Int. Ed. Engl.*, **33**, 223 (1994).

55) M. Kurmoo, A. W. Graham, P. Day, S. J. Coles, M. B. Hursthouse, J. L. Caulfield, J. Singleton, F. L. Pratt, W. Hayes, L. Ducasse, and P. Guionneau, *J. Am. Chem. Soc.*, **117**, 12209 (1995).

56) M. Kurmoo, P. Day, P. Guionneau, G. Bravic, D. Chasseau, L. Ducasse, M. L. Allan, I. D. Marsden, and R. H. Friend, *Inorg. Chem.*, **35**, 4719 (1996).

57) H. Kobayashi, H. Tomita, T. Naito, A. Kobayashi, F. Sakai, T. Watanabe, and P. Cassoux, *J. Am. Chem. Soc.*, **118**, 368 (1996).

58) M. M. Shieber, "Experimental Magentochemistry—Nonmetallic Magnetic Materials," Amsterdam, North-Holland, (1967).

59) E. M. Kosower, R. L. Martin, and V. W. Meloche, *J. Am.*

Chem. Soc., **79**, 1509 (1959).
60) H. Kobayashi, T. Udagawa, H. Tomita, K. Bun, T. Naito, and A. Kobayashi, *Chem. Lett.*, **1993**, 1559.
61) A. Kobayashi, T. Udagawa, H. Tomita, T. Naito, and H. Kobayashi, *Chem. Lett.*, **1993**, 2179.
62) A. Bondi, *J. Phys. Chem.*, **68**, 441 (1964).
63) M. Enomoto, A. Miyazaki, T. Enoki, and G. Saito, private communication.
64) H. Tanaka, F. Tsuruoka, T. Ishii, H. Izumi, K. Iio, and K. Nagata, *J. Phys. Soc. Jpn.*, **55**, 2369 (1986).
65) I. Dyzaloshinsky, *J. Phys. Chem. Solids*, **4**, 241 (1958).
66) T. Moriya, *Phys. Rev. Lett.*, **4**, 228 (1960).
67) C. Faulmann, P. Cassoux, E. B. Yagubskii, and L. V. Vetoshkina, *New. J. Chem.*, **17**, 385 (1993).
68) E. B. Yagubskii, A. I. Kotov, E. E. Laukhina, A. A. Ignatiev, L. I. Buravov, A. G. Khomenko, V. E. Shklover, S. S. Nagapetyan, and Yu. T. Struchkov, *Synth. Met.*, **41-43**, 2515 (1991).
69) O. A. Dyachenko, V. V. Gritsenko, G. V. Shilov, E. E. Laukhina, and E. B. Yagubskii, *Synth. Met.*, **58**, 137 (1993).
70) J. Yamaura, K. Suzuki, Y. Kaizu, T. Enoki, K. Murata, and G. Saito, *J. Phys. Soc. Jpn.*, **65**, 2645 (1996).
71) T. Mori, F. Sakai, G. Saito, and H. Inokuchi, *Chem. Lett.*, **1987**, 927.
72) P. Guionneau, G. Bravic, J. Gaultier, D. Chasseau, M. Kurmoo, D. Kanazawa, and P. Day, *Acta Crystallogr., Sect. C*, **C50**, 1894 (1994).
73) M. Watanabe, Y. Nogami, K. Oshima, J. Yamaura, T. Enoki, and G. Saito, *Solid State Commun.*, **100**, 755 (1996).
74) L. J. de Jongh and A. R. Miedema, *Adv. Phys.*, **23**, 1 (1974).
75) R. Tsuchiya, S. Yoshizaki, T. Nakamura, T. Takahashi, J. Yamaura, K. Suzuki, T. Enoki, and G. Saito, *Synth. Met.*, **70**, 967 (1995).
76) J. Yamaura, T. Enoki, H. Takahashi, and N. Mouri, private communication.
77) D. Chasseau, P. Guionneau, J. Gaultier, Y. Barrans, L. Ducasse, C. J. Kepert, P. Day, and M. Kurmoo, *Synth. Met.*, **86**, 2045 (1997).
78) M. Watanabe, Y. Nogami, K. Oshima, J. Yamaura, T. Enoki, and G. Saito, private communication.
79) J. R. Marsden, M. L. Allan, R. H. Friend, M. Kurmoo, D. Kanazawa, P. Day, G. Bravic, D. Chasseau, L. Ducasse, and W. Hayes, *Phys. Rev.*, **B50**, 2118 (1994).
80) F. Keffer, "Encyclopedia of Physics," ed by H. P. J. Wijn, Springer Verlag, Berlin (1966), Vol. XVIII/2, p. 124.
81) J. Yamaura and T. Enoki, private communication.
82) H. Kobayashi, A. Miyamoto, R. Kato, F. Sakai, A. Kobayashi, Y. Yamakita, Y. Furukawa, M. Tasumi, and T. Watanabe, *Phys. Rev.*, **B47**, 3500 (1993).
83) T. Tamura, Y. Kashimura, H. Sawa, S. Aonuma, R. Kato, and M. Kinoshita, *Solid State Commun.*, **93**, 585 (1995).
84) M. Tokumoto, T. Naito, H. Kobayashi, A. Kobayashi, V. N. Laukhin, L. Brossard, and P. Cassoux, *Synth. Met.*, **86**, 2161 (1997).

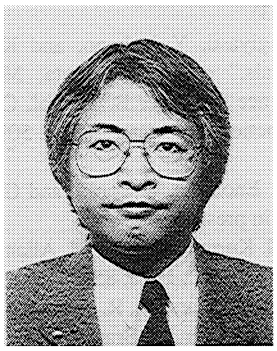

Toshiaki Enoki was born in 1946 in Gunma, Japan. He received his B. Sc. degree in 1969, M. Sc. in 1971 and D. Sc. in 1975 from Kyoto University. He joined the Institute for Molecular Science as a research associate in 1977. He was appointed as associate professor of the department of chemistry at Tokyo Institute of Technology in 1987, and he was promoted as full professor in 1990 in the same university. His current interests include solid state chemistry, especially electronic and magnetic properties of organic solids and carbon materials.

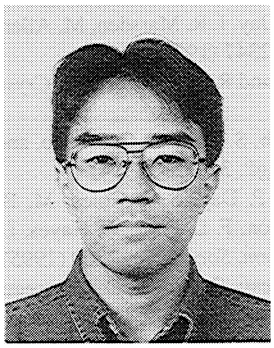

Jun-Ichi Yamaura was born in 1969 and raised in Saitama, Japan. He received his Ph. D degree in chemistry under the direction of Prof. T. Enoki from Tokyo Institute of Technology in 1997. In April 1997, he was appointed as research associate in the Institute for Solid State Physics in The University of Tokyo. His research interests include electronic and magnetic properties of organic charge transfer complexes.

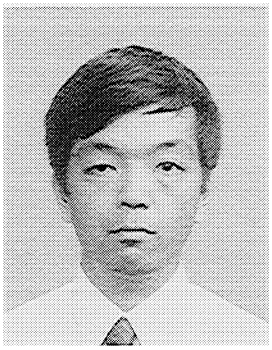

Akira Miyazaki was born in 1966 in Niigata, Japan and raised in Tochigi. He received his M. Sc. degree from The University of Tokyo in 1991 and he was educated in the doctoral course at the same university. Since October 1993 he has been a research associate of the department of chemistry at Tokyo Institute of Technology. His current research interests include the study of transport and magnetic properties, phase transition mechanism of molecular conductors.